Investigation of Basic-acid Site Properties on Catalytic Depolymerisation of Nylon-6

A Study on Metals and Metal Oxide Supports

Master's thesis in Materials Chemistry

Gabriel Samuelsson

DEPARTMENT OF Chemistry and Chemical Engineering

CHALMERS UNIVERSITY OF TECHNOLOGY

Gothenburg, Sweden 2025

www.chalmers.se

MASTER'S THESIS 2025

Investigation of basic-acid site properties on catalytic depolymerisation of Nylon-6

A Study On Metals and Metal Oxide Supports

Gabriel Samuelsson

CHALMERS
UNIVERSITY OF TECHNOLOGY

Department of Chemistry and Chemical Engineering
Division of Chemical Processes and Reaction Engineering, KART
CHALMERS UNIVERSITY OF TECHNOLOGY
Gothenburg, Sweden 2025

Investigation of basic-acid site properties on catalytic depolymerisation of Nylon-6
A Study on Metals and Metal Oxide Supports
Gabriel Samuelsson

Supervisor: Prabin Dhakal, Department of Chemistry and Chemical Engineering
Examiner: Derek Claude Creaser, Department of Chemistry and Chemical Engineering

Master's Thesis 2025
Department of Chemistry and Chemical Engineering
Division of Chemical Processes and Reaction Engineering, KART
Chalmers University of Technology
SE-412 96 Gothenburg
Telephone +46 31 772 1000

Cover: Separation of caprolactam after hydrogenative depolymerisation reaction using nylon 6

Typeset in LaTeX
Printed by Chalmers Reproservice
Gothenburg, Sweden 2025

Investigation of basic-acid site properties on catalytic depolymerisation of Nylon-6

A Study On Metals and Metal Oxide Supports

Gabriel Samuelsson

Department of Chemistry and Chemical Engineering

Chalmers University of Technology

Abstract

In the last 100 years, plastic pollution has become a huge issue, with over 350 million tonnes of waste generated each year. Heterogeneous catalysis of plastic waste represents a promising alternative to conventional recycling methods, yet remains rather undeveloped, particularly for polyamides, such as nylon-6.

The purpose of the study was to investigate the effect of the basic and acid sites of the incorporated metal oxides of MgO, SrO, WO_3, La_2O_3, Y_2O_3 and MnO_x for the hydrogenative depolymerisation reaction of nylon 6 to ϵ-caprolactam using a Ru/ZrO_2 based catalyst. The work was carried out by investigating both co-precipitated and commercial ZrO_2 based catalysts, using several analysis methods to characterize the catalysts and reaction products.

The results of the study showed that the commercial ZrO_2-based catalysts, compared to the co-precipitated catalysts, exhibited higher surface areas, increased pore volume and average pore diameter, as well as a large increase in basicity and acidity, likely due to improper precipitation, as shown by the ICP-MS results. The conversion of nylon-6 was shown to not vary greatly between the two different catalysts, however, for some commercial ZrO_2-based catalysts, the conversion decreased by up to 40%, while the SrO-based catalysts showed up to double conversion compared to the Ru/ZrO_2 catalyst.

The most effective catalyst was found to be the Ru/10SrO-ZrO_2 catalyst, with a nylon-6 conversion of 42,4% and 33,8% ϵ-caprolactam yield. The effectiveness was likely related to the high degree of strong basic sites present on the surface of the catalyst and possibly the perovskite $SrZrO_3$ structure, however further studies of this phenomenon and possibly increased ruthenium loading were suggested to further improve the catalyst.

Keywords: Plastic waste, Sustainability, Depolymerisation, Nylon-6, Hydrogenation, Catalysis, ϵ-Caprolactam

Acknowledgements

The research presented in this thesis was conducted mainly at the division of chemical engineering, Competence Center of Catalysis (KCK), and partly in the Chalmers Materials Analysis Laboratory (CMAL), Chalmers University of Technology, Gothenburg, Sweden and took place between January 2025 and June 2025.

This project would not have been possible without the great mentorship of my supervisor, Prabin Dhakal, who has guided me throughout this thesis project, introduced me to advanced analytical instruments, remained patient during my stupid questions and always provided assistance when needed. My deepest gratitudes to Professor Louise Olsson and my examiner Professor Derek Creaser for the opportunity to perform my master's thesis at the Division and for the help and insight provided into chemical engineering.

I would also like to thank all fellow master's and international internship students for keeping me company during these 5 months and proving a good way to help in the process with the discussion of topics, methodologies, and analysis methods as well as giving tips on efficient writing.

I am really fortunate to have been part of such a friendly workplace for my master thesis. I would specifically like to acknowledge Johanna Spång for providing excellent administrative support, Michael Andersson-Sarning for providing an excellent introduction to laboratory safety guidelines, and providing a safe and learning environment. As a special thank you, I would also like to thank Wei Di, Mütesir Temel, Aladdin Mardanov, Muhammed Imran, Vikash, Katherine Louise Barber, Johan Nilsson, Jia Wei Chew, Rawipa Intakul, Elham Nejadmoghadam, and Aqsa Noreen for providing a positive, encouraging workplace and insights into your cultures. You all made this at least 10 times more fun and inspiring than anticipated.

Lastly, I'd like to thank my parents, Petra and Christer, for providing a safe and encouraging environment, as well as my friends and family, who are always there when I need a break from studying or when I simply need to rant about my latest exam.

Gabriel Samuelsson, Göteborg, June 2025

List of Acronyms

BET	Brunauer-Emmett-Teller
BJH	Barret-Joyner-Halenda
CL	Caprolactam
CMAL	Chalmers Materials Analysis Laboratory
DMT	DiMethyl Terephthalate
DRIFTS	Diffuse Reflectance Infrared Fourier Transform Spectroscopy
DSC	Differential Scanning Calorimetry
EG	Ethylene Glycol
FID	Flame Ionization Detector
GC	Gas Chromatography
HDPE	High-Density PolyEthylene
ICP	Induced Coupled Plasma
IS	Internal Standard
IWI	Incipient Wetness Impregnation
LSZ	Lanthanum-Stabilized Zirconia
LDPE	Low-Density PolyEthylene
MALDI	Matrix-assisted laser desorption/ionization
MOP	Metal-Oxide-Polymer
MS	Mass Spectrometer
PA	PolyAmides
PE	PolyEthylene
PEG	Poly-Ethylene Glycol
PET	PolyEthylene Terephthalate
PP	PolyPropylene

PS	PolyStyrene
PTA	(Para)-Terephthalic Acid
PU	PolyUrethane
PVC	PolyVinyl Chloride
SSA	Specific Surface Area
TCD	Thermal Conductivity Detector
TOF	Turn Over Frequency
TPD	Temperature-Programmed Desorption
TPR	Temperature-Programmed Reduction
TGA	Thermogravimetric Analysis
XPS	X-ray Photoelectron Spectroscopy
XRD	X-ray Diffraction
YSZ	Yttrium Stabilised Zirconia

Contents

List of Figures

List of Tables

1

Introduction

Due to their versatility, cost effectiveness, and durability, plastic polymer materials have become indispensable in modern society. However, end-of-life mismanagement has caused major environmental challenges, resulting in lasting ecological damage of approximately 350 million tonnes of plastic waste produced every year [1], and high economic costs as a result of the take-up of high pollution control measures required.

1.1 Plastics

In essence, plastics, both industrial and commercial, are different forms of synthesized polymers, consisting of repeated smaller building blocks, also known as monomers, forming high molecular weight polymers with the occasional branches or functional groups. As a result of the immense variability of synthetic polymer structures, an almost endless amount of polymers can be synthesized and optimized to fit the needs of the material and environment in which they will be used. The most common synthetic polymers include polyethylene (PE), which includes both high-density polyethylene (HDPE) and low-density polyethylene (LDPE), polyethylene terephthalate (PET), polyvinyl chloride (PVC), polyamides (PA), polypropylene (PP), polystyrene (PS), and polyurethane (PU). A selection of synthetic polymers, including the molecular structure of PE, PET and PVC, are shown in Figure 1.1.

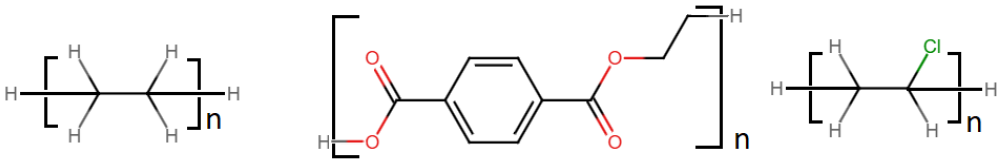

Figure 1.1: Commonly used commercial polymers, showing the molecular structures of PE, PET, and PVC

One of the first discoveries of synthetic polymers was made in 1869 by John Wesley Hyatt, as a substitute for ivory, due to the diminishing supply of naturally sourced ivory from wild elephants [2]. This polymer, named celluloid, was made by treating cellulose made from cotton fibre with camphor, resulting in a material that can be processed to mimic natural polymers and substances like tortoiseshell, horn, linen, and ivory [2].

A truly synthetic polymer took more years to develop. Not until 1907, a man named Leo Baekeland invented Bakelite, the first fully synthetic polymer, free from any natural raw materials, marketed as "the material of a thousand uses" [2]. This polymer was made as a substitute for shellac, a natural electrical insulator, to meet the needs of the electrification of the United States.

Hyatt's and Baekeland's major success caused a global rush in the development of new synthetic polymers [2]. Although Hyatt and Baekeland polymers were created for a suitable task, new research and development was instead focused on creating new polymers and then finding uses for them later [2]. Years later, in modern-day society, thousands of plastic polymer varieties have emerged and can now be found anywhere you look.

In many communities and developing countries around the world, recycling infrastructure simply does not exist and the economic incentive to recycle does not prevail. As a result of plastic production increasing by an average of 8% every year from 1950-2022 [3], the amount of plastic waste has also far exceeded the recycling capabilities of modern society. In 2019, an average of only 9% polymers out of 350 million tons of plastic waste worldwide were being recycled and $\approx$ 22% improperly disposed of, often disposed in improper landfills, bodies of water or as littering [4]. These problems become more obvious in developing countries, where plastics offer a cheap way to develop without the waste management capabilities of developed countries.

Due to the large amount of improperly disposed waste and large amounts of landfill waste, a better system for profitable recycling must be implemented.

1.2 Waste management

One of the widely available plastic recycling methods, developed as a response to current problems we face, is mechanical recycling, which deals primarily with post-consumer waste in a closed-loop system or post-industrial waste in a open-loop or semi-closed loop [5]. Mechanical recycling, where common methods include thermal extrusion, is the use of thermal conduction and viscous shearing to induce thermal softening or plasticization, and producing extrudes. However, thermal conduction and viscous shearing also causes thermo-oxidative and sheer induced chain degradation [5]. Mechanical recycling also struggles with impurities in the form of mixed polymer blends [5]. Mixed polymer blends cause fractures in the extrudes and phase separation as a result of melt incompatibility, causing major inefficiencies in the recovery and reuse of plastic waste, as well as ineffective transfer of stress and strain across phase boundaries, causing degraded mechanical properties with each recycling cycle [5]. As a result of degradation of mechanical properties, the number of times a material can truly be recycled is limited, often limited to three to five times, which in turn truly limits the scope and possibilities of a circular economy [5]. These inefficiencies have led researchers all over the world to explore alternative recycling methods and improvements to existing technologies for increased sustainability and effectiveness. Due to the requirements of pure polymer blends in the feedstock, extensive plastics sorting is required, and this is one of the reasons why PET recycling is mostly successful, while other plastics struggle [5].

Chemical recycling methods, including methods such as pyrolysis, hydrolysis, and aminolysis, are some of the alternatives to mechanical recycling. However, these methods often involve low selectivity due to char formation and critical product separation (pyrolysis), harsh reaction conditions with high-pressure gas / solvents, acid / basic catalysts (hydrolysis and aminolysis) and potential negative environmental impact of solvents (hydrolysis and aminolysis) [6][7]. Due to the problems of current commercial chemical recycling methods, newer and greener recycling methods have been investigated to increase selectivity and yield using less harsh conditions and solvents [6]. Catalytic depolymerisation of plastics is one promising method due to the characteristics of catalysts, causing a lower reaction energy barrier and contributing to lower energy

use, offering a way for all countries to increase their recycling capabilities. One polymer with specific focus is polyamides, specifically nylons, commonly found in fishing equipment, ropes, and certain automotive parts, which cause a great deal of oceanic pollution and harm to aquatic lifeforms, one of the major problems of current waste mismanagement, causing disruptions in aquatic ecosystems.

One method currently investigated is the reductive depolymerisation of aliphatic polyamides, the market is mainly represented by nylon-6 and nylon-6,6 polymers [8], using hydrogen as a reducing agent accompanied by a catalyst for more efficient depolymerisation. Only a few of these have so far emerged, the most promising being the homogeneous catalytic reductive depolymerisation of nylon-6 and amides, using the ruthenium pincer catalyst [8]. However, homogeneous catalysis suffers from the problems of catalyst reuse, product separation, etc., and does not directly form ϵ-caprolactam, instead it forms alcohols and amines. To avoid the product separation costs of homogeneous catalytic reaction, enable polymer to monomer recycling, and maximize the selectiveness and yield of ϵ-caprolactam, heterogeneous catalysis methods have been investigated using the active metal catalyst ruthenium on supported zirconia (Ru/ZrO_2) as a way to reduce the cost of product separation using homogeneous catalysis [9]. The investigation was related to optimizing the reaction conditions using the Ru/ZrO_2 catalyst. Due to the success of the study, the effects of modifications to catalyst support will be investigated to potentially increase the conversion of nylon-6 to ϵ-caprolactam using reductive catalytic depolymerisation.

1.3 Aim

Based on the Ru/ZrO_2 catalyst, the aim of the study is to examine whether modifications, mainly affecting acidity and basicity, in the form of different ZrO_2 support compounds, can alter the catalytic activity of the catalyst used for the reductive catalytic depolymerization of nylon-6. Specifically, this is done by investigating whether the choice of metal oxide inclusions, including Mg, Sr, W, Y, La, and Mn oxides in zirconia-based composites affects the characteristics, reactivity, and effectiveness of the catalyst. Using the results of the study makes it possible to further develop industrial processes for catalytic recycling and add to the database of information available for future studies.

1.4 Specification of the issue being investigated

Due to the limited studies on catalytic hydrogenation depolymerisation reactions of nylon-based polymers, as previously reported, the aim of the study was to investigate the acidity/basicity and how the support characteristics affect the catalytic activity.

The following questions are to be answered during the thesis: How does the microstructure of the support affect the properties of the catalyst; How does the ratio of different metal oxides affect the microstructure of the support and properties of the finalized catalyst; To what extent does basicity and acidity of the catalyst affect depolymerisation of nylon-6 and; Is the hydrogenative depolymerisation of nylon-6 using Ru/MO_x-ZrO_2-based catalysts a valid catalytic depolymerisation method worthy of further research.

2

Theory

Noble-metal catalysts are generally expensive to produce or buy, so the improvement and maximization of the catalytic activity for the given task are required. This is done by varying the chemical structure and identity of the support structure and any dopants such as promoters or inhibitors. The characteristics of the support materials are crucial to the given situation; an example of this is the porosity of the support, which limits the polymer chain length that makes contact with the active metal particles in the pores of the support. Other characteristics, such as surface roughness and surface species, including promoters and inhibitors, are also crucial when designing the catalyst. Metal-support interactions are also crucial in the design of the catalyst; Stronger interactions may reduce the activity of the catalyst or increase selectivity towards reactions that require such specifications, while weak interactions could cause too reactive active metal particles, reducing the selectivity of the reaction or allowing more non-reactive reactions [10].

These are merely a few examples of the characteristics that are critical when designing catalytic particles for use in chemical reactions. The design process of a catalytic reaction is inherently time-consuming as a result of the incredible amounts of catalyst combinations available, which necessitates multiple experiments and characterization techniques to identify an optimal approach.

When dealing with depolymerisation reactions, controlling the pore sizes of the catalytic material is crucial. A slight modification of the catalytical particle structure or support composition can cause vast differences in effective surface area and pore diameter [11]. In a study reported by *Cisneros et al.* [11], the introduction of MgO doping on ZrO_2 supports caused the pore diameter to reduce to almost half its size and an increase of 50% in the specific surface area (SSA). The high surface area indicates that the metal loading can be performed in a highly dispersed manner, where each active metal particle will expose the maximum of its surface area

to reactants, increasing the turn-over frequency (TOF) of the catalyst [12]. The support structure also increases thermal stability and prevents loss of surface area due to sintering over time of unsupported active metal catalysts [12]. The increase in SSA logically also increases the reaction rates and conversion of reactants as a result of the higher TOF of higher surface area active metal particles [12], allowing higher capacities and therefore increased feed flow in a potential continuous reactor. This is possible because of the increased reaction kinetics of larger surface-area catalysing particles.

On the other hand, the composition of the catalyst system significantly influences the surface properties of the material. A study on CO_2-TPD conducted by *Miyamoto et al.* [13] demonstrated that, for the Ru/Mg-La-ZrO_2 and Ru/Sr-La-ZrO_2 catalysts, there was quite a difference in number and characteristics of basic sites. The higher amount of CO_2 desorption (in μmol/g) of the Ru/Mg-La-ZrO_2 catalyst indicated that there was a greater number of basic sites on the surface area of the support. These differences provide clear evidence of the distinct basic sites present in each catalyst and demonstrate how the incorporation of metal oxides influences the surface characteristics of the catalyst.

2.1 Catalysis

The most important aspect of improving chemical reactions on the industrial scale is making them efficient, both in terms of conversion and profitability. Catalysts are one of the most important factors in the design of chemical reactions because of their inherent ability to lower the activation energy of the reaction and increase the selectivity toward the desired reaction pathways [14]. These facts make them more efficient in terms of the reduction in energy required and minimizing waste [14]. Catalysts come in many shapes, such as in pellets or in solutions, the former being used mainly in heterogeneous catalysis, while the latter are used mainly in homogeneous catalysis.

Having both reactants and catalyst in the same phase, liquid reactants in acidic / base solutions commonly refer to homogeneous catalysis. Homogeneous catalysis reactions are generally more efficient than reactions using heterogeneous catalysis because of the homogeneous nature of the reaction mixture, allowing greater control and selectivity [15]. However, the product mixture will require possibly extensive and/or expensive separation methods to obtain rela-

tively pure products, contributing to the cost of operation for operating homogeneous catalytic reactions.

2.1.1 Heterogeneous catalysis

As a result of the disadvantages of homogeneous catalysis, heterogeneous catalysis has been used to study the feasibility of catalytic depolymerisation of nylon 6. Heterogeneous catalysis is the reaction in which the reactants and catalyst are of a different phase, e.g. solid catalysts with liquid phase reactants or solid catalysts with gas phase reactants. Heterogeneous catalysed reactions generally have easier separation of the products from reactants and catalysts than homogeneous catalysed reactions, often requiring as little as a filtration setup or similar methods to isolate the product from unreacted reactants, allowing for easier reuse of catalysts [15]. However, this method has a huge flaw, mainly in the limitation of mass transfer that causes inefficiencies in the reaction kinetics. This is one of the reasons why different solvents and intense stirring are used to try and increase the mass transport.

In Heterogeneous catalysis, some of the commonly used methods of catalysing reactions are the loading of reduced active metals, often metals such as Ru, Pt, Pd, Fe, Co, or Ni, on zeolites or metal oxide supports. The reduced active metal reduces the activation energy of the reaction by forming stabilized intermediate phases, allowing for more reaction pathways. To prevent sintering of the active metal, the active metal is often used together with a support material, any thermally stable porous structures providing a large surface area, such as alumina, silicate or zirconia [10]. One of the most important additions to metal oxide support catalysts is the inclusion of inhibitors and promoters, which alters the reactivity and selectivity of the active metal site [16]. Inhibitors generally decrease the activity of the active metal, as well as change the selectivity towards certain reaction paths or remove intermediates and bi-products, causing a change in the reaction kinetics, possibly favouring another reaction path and changing the reaction selectivity [16]. Promoters, on the other hand, although generally inert by themselves, increase the activity of nearby active metal sites, often by donating or removing electrons, causing an increase in activity. This may not always be preferable because of the changes in selectivity, but a combination of inhibitors and promoters can create really specific reaction pathways. For example, the Haber-Bosch synthesis process, in which reduced iron is used, is often promoted by K_2O, alumina, or CaO [17].

2.2 Nylon 6 polymerisation

Nylon 6 is a highly versatile polymer commonly used in textiles, packaging materials and, in some capacities, industrial applications such as tires, hoses, and belts [18]. The polymerization reaction, turning ϵ-caprolactam into nylon 6 is usually carried out in a slightly acidic water solution or using an anionic initiator, a strong base, such as NaOH in an anhydrous environment [18]. Because of the anhydrous conditions required for anionic initiated polymerization reactions and the difficulties that these present, industrial polymerization reactions are most likely to be carried out by hydrolytic reaction mechanics. The continuous reaction, as described by *Hu & Yang* [18], is commonly initiated at 230-240°C and the chain growth stage proceeds at temperatures of 260°C.

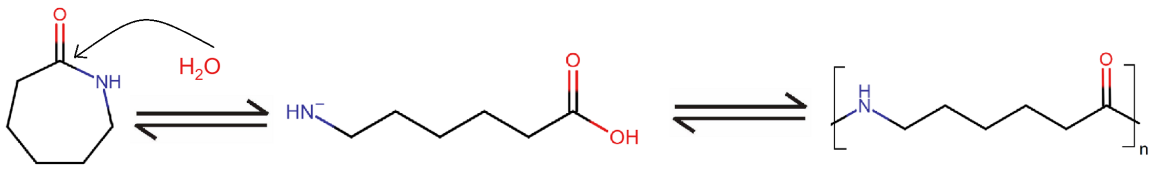

Figure 2.1: General polymerization reaction of ϵ-caprolactam. The reaction mechanisms follows a fairly standard ring-opening polymerization process. A polymer of length n requires n ϵ-caprolactam molecules.

A similar reaction to the reverse reaction in Figure 2.1, without forming excess water and using H_2 will be studied, transforming the nylon 6 polymer into its monomeric counterpart: ϵ-caprolactam, commonly referred to as a depolymerisation reaction. Although there are some recycling methods currently commercially available for different types of polyamides, most of them use quite harsh reaction conditions, as described in Section 1.2, and only a few stud-

ies have been performed on more sustainable recycling methods, such as the hydrogenative catalytic depolymerisation of nylon 6 [19]. This patented study was optimized using the homogeneous Ruthenium pincer catalyst, KO-tert-butyl (8mol%), 70 bar of H_2, and 150°C for 48 h, resulting in 77 80% conversion of nylon-6 (resins) and formation of 6-amino-1-hexanol in 24–26% yield [19]. Although this study was relatively successful, the industrial synthesis of nylon-6 and other nylons uses caprolactam as feedstock as opposed to 6-amino-1-hexanol, making this process unsuitable for the re-polymerization of nylons.

2.3 Catalyst preparation methods

Because of the wide range of catalysts available on the market and the specific characteristics required for every reaction, the vast majority of industrial catalytic applications are different from each other. Although common in some industries, one size fits all rarely applies in the field of catalysis. As a result of the complexity of catalytic systems, multiple preparation methods exist to accommodate the specific properties desired. One of the promising catalysts to investigate is the Ru/MO_x-ZrO_2 catalyst due to the previous success of using unmodified Ru/ZrO_2 in hydrogenative catalytic depolymerisation of Nylon-6 [9]. Some of the common methods, which were used in this study, are incipient wetness impregnation and co-precipitation methods.

2.3.1 Co-precipitation

Co-precipitation is one of the methods used to prepare supported catalysts; however, it was mainly used for support preparation during this work and thus required another method to finalize the catalyst, the incipient wetness impregnation described below. The supports are prepared by using two or more metal oxide precursors and dissolving them in a solution together with the optional polymer or surfactant, which is sometimes used to form a template by surfactant self-assembly, in which the catalyst structure can easily take shape. The precipitation is then formed by changing the solubility criteria of the new metal oxide polymer (MOP) structure by a precipitation agent, commonly done by changing the pH of the solution. The precipitation is then easily filtered to form an almost ready-to-use support structure [11]. To finalize the support, it needs to be dried in an oven and calcined to burn the template, forming the desired porous structure.

2.3.2 Incipient wetness impregnation

Incipient wetness impregnation, also known as dry impregnation, is a catalyst preparation method in which a catalyst precursor solution is absorbed into a pre-fabricated support structure, using capillary forces to fill the pore volume of the support material. In contrast to wet impregnation, where the impregnation volume is larger than the pore volume, dry impregnation is designed in such a way that the volume of the precursor solution does not exceed the volume of the pores of the support. This reduces the need for recycling or handling excess precursor solution waste produced by wet impregnation methods [20]. Limited liquid filling also eliminates the need for filtration, but also leaves counterions, commonly Cl ions, nitrates or sulfates as residual from the precursor salt, on the surface of the support material, sometimes even after calcination [20][21].

Precursor salts can look vastly different depending on which chemical or metal is required during impregnation. In the case of ruthenium, ruthenium(III) nitrosyl nitrate was used, while zirconia support precipitated from zirconyl nitrate hydrate was used instead, both of which contain nitrates, making it generally easier to remove via calcination. Ruthenium(III) nitrosyl nitrate, a salt that forms nitrosyl nitrate counterions; compared to chlorides and sulfates, it is not retained and is marginally easier to remove [21]. Chloride ions are also known to inhibit and deactivate active metal sites, causing a reduction in catalytic activity. Therefore, the choice of precursor salt and preparation method is crucial to obtain the desired result [21].

2.4 Characterisation methods

When dealing with any type of research or project, the characterization of the results is a vital part of understanding why the result turned out the way it did, why it works, or how it could have been improved. Factors such as catalyst structure, surface area, surface species, porosity, basicity, acidity, metal-support interactions, and morphology are of huge interest within catalysis. To investigate these characteristics of prepared catalytic particles, numerous methods including XRD, N_2-physisorption, NH_3-TPD, CO_2-TPD, H_2-TPR, and CO/CO_2-DRIFTS can be utilized to derive the properties of catalytic systems and chemical reactions.

2.4.1 N_2 physisorption

The N_2-Physisorption analysis method is a methodology developed to measure the porous properties of materials, mainly SSA, as well as the pore volume and average pore size distributions. This is done by measuring the nitrogen adsorption properties of the material during filling and emptying of the pores. In the instrument, this is done by an increase, accompanied by a corresponding decrease in nitrogen pressure in the specially designed sample tubes. The measurements are taken at -196°C, the boiling point of nitrogen. This low temperature reduces the kinetic energy of the adsorbate, facilitating easier adsorption of N_2.

The BET theory is an extension of Langmuir theory, the theory behind monolayer molecular adsorption in the way of modulating multilayer molecular adsorption [22]. The BET theory is thus based on the following assumptions: Gas molecules physically adsorb on a solid in layers infinitely; gas molecules only interact with adjacent layers, and the Langmuir theory can be applied to each layer; the enthalpy of adsorption for the first layer is constant and greater than the second (and higher); the enthalpy of adsorption for the second (and higher) layers is the same as the enthalpy of liquefaction [23]. The resulting theory of multilayer adsorption yields the isotherm. Together with the isotherm and the BET equation, shown in Equation 2.1, where factors such as equilibrium pressure, saturation pressure, and amount of adsorbed gas are used together with the isotherm, the SSA of the catalyst can be obtained using the known value of the volume of N_2.

$$\frac{p}{v(p_0 - p)} = \frac{1}{v_m c} + \frac{c-1}{v_m c}\frac{p}{p_0} \tag{2.1}$$

The plot of the data obtained from the physisorption instrument yields the isotherm adsorption plot, where the volume of N_2 adsorbate is plotted against the relative pressure. As the keen-eyed ones might notice from equation 2.1, the equation can be plotted linearly using $y = \frac{p}{v(p_0-p)}$ and $x = \frac{p}{p_0}$ as shown in figure 2.2. This allows the calculation of intersects and slopes to obtain the volume of a monolayer and the BET constant, c, according to the formulae illustrated in Figure 2.2.

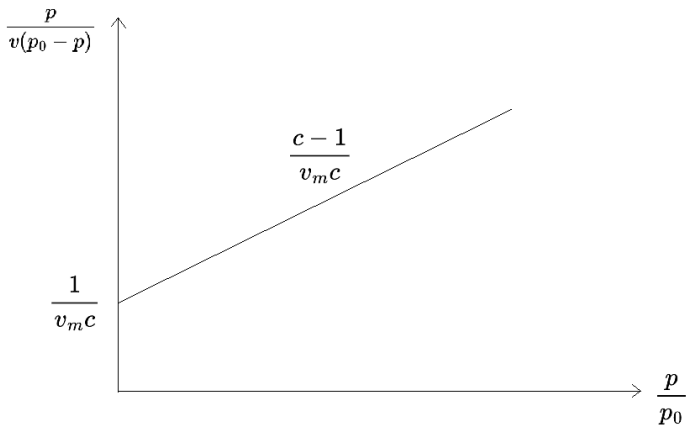

Figure 2.2: A general representation of the linearisation of the BET equation

Now, when the monolayer volume of N_2 is known, using fairly standard physical sizes of the N_2 molecule, the surface area of the sample can be calculated. This is usually performed by the instrument during measurement, but the data can also be manually plotted and calculated to obtain the surface area.

2.4.2 X-Ray Diffraction

As a result of the high intensity energy, X-ray diffraction (XRD) is a methodology used to study the crystallographic structure of solid samples. As a result of their uniform spacing, diffraction patterns can be spotted from incident X-ray beams [24]. These x-rays, as a result of a wavelength that matches closely with the interatomic distances in most crystal structures, cause diffractions in wave patterns with x-rays diffracted from secondary atomic layers, as illustrated in Figure 2.3. This is only possible because of the highly periodic order of crystalline materials, and any attempts at recreating with amorphous materials would only result in destructive interference and thus no characteristic signals [24]. The amount of diffraction changes based on the incident angle of the X-rays, and at one such angle, the diffraction would cause constructive interference intensifying the signal obtained. This constructive interference gives information on the crystal lattice and is illustrated in Figure 2.3. Using this information obtained together with Bragg's law, the distance between lattice planes can be calculated, and the identity of the material can be determined.

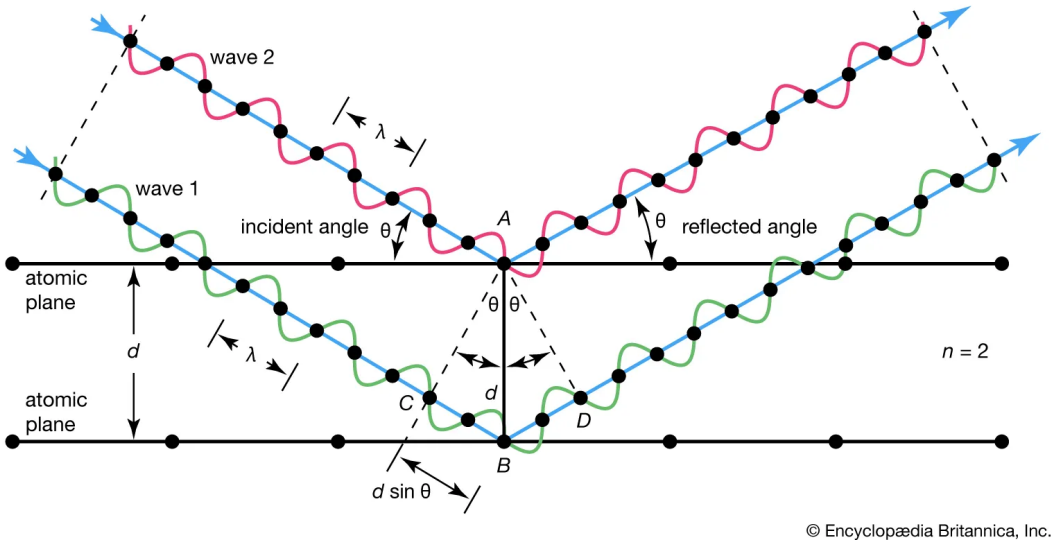

Figure 2.3: Two waves, in phase with each other gets reflected by atom A and B. Due to the specific inclination angle the phase shifted wave is shifted by exactly two wavelengths, causing a peak in the diffraction pattern as illustrated.

By courtesy of Encyclopædia Britannica, Inc., copyright 2002; used with permission.

2.4.3 Temperature-programmed studies

Temperature-programmed studies, commonly including CO_2-TPD to measure the basicity of a surface material and NH_3-TPD to measure the acidity of a surface, are characterization techniques used to determine the amount of acid / basic sites present on a surface or support structure. The acid and base sites are characterized by the adsorption of the adsorbate on the surface, slowly increasing the temperature while monitoring the CO_2 desorption using a MS to determine at what temperature the adsorbate desorbs, indicating the strength and the number of acidic or basic sites [25]. Acidity and basicity are often represented by the Lewis-Brønsted theories of acidity and basicity. Both the Lewis theory and Brønsted theory explain the acid/base properties of material surfaces through the reduction and oxidation mechanisms of functional groups. The formal definition of an Brønsted acid and base is such that, when reacted together, it forms their respective conjugated base and conjugated acid [25], as shown in equation 2.2. A represents a general Lewis acid, such as a carboxylic acid or an alcohol, while B represents a general Lewis base, such as ammonia or NaOH. Water can also be classified as both a Lewis acid and a base, due to its self-ionization properties, forming both OH^- and H_3O^+ in small quantities, as shown in Equation 2.3.

$$AH + B \leftrightharpoons A^- + BH^+ \tag{2.2}$$

$$H_2O + H_2O \leftrightharpoons OH^- + H_3O^+ \quad K_w = 10^{-14} \tag{2.3}$$

An acidic site is characterized as a functional group capable of donating a proton (Brønsted acid) or receiving an electron pair (Lewis acid), effectively reducing the functional group [25]. The hydroxyl groups (-OH) are present at Brønsted acid sites, -OH being able to donate a proton, effectively reduced to O^-, while one of the simplest Lewis acids, the hydrogen ion, also known as a proton, can accept an electron pair from any lone electron pair, commonly found in the ammonia molecule (NH_3), or similar molecules such as OH^-, forming the ammonium ion (NH_4^+) or H_2O.

On the other hand, a basic site is characterised as a functional group being able to accept protons (Brønsted base), such as the ammonia or hydroxide groups [25] mentioned previously. A basic site can also be characterized as an electron pair donor, such as O^- or O^{2-}.

On catalyst support surfaces, acidic sites are commonly illustrated by M-OH functional groups, which are able to donate a proton, forming M-O^-. Acidic sites can be detected and quantified using any Lewis base, such as ammonia, where NH_3-TPD is a good method for this characterization. A basic site often consists of oxygen anions (O^{2-}), which are capable of accepting protons or donating electron pairs. A common Lewis acid CO_2, which is capable of detecting and characterizing basic sites by accepting an electron pair, is commonly used in characterization techniques such as CO_2-TPD, described above. The NH_3-TPD and CO_2-TPD analysis methods are chosen because of their ease of availability, low cost of adsorbate and small molecular sizes selectively adsorbing onto the basic and acidic sites.

Reduction of metal oxide catalysts is another important aspect to consider for the characterization of metal oxide catalyst supports. Reduction is an important step in the process of creating reactive and active metal sites for use during any reaction. Reduction of metal oxides using molecular hydrogen is a multistep process that involves the general removal of oxygen from the crystalline matrix of the oxide and is driven by the formation of H_2O [26]. The process starts with the adsorption and dissociation of molecular hydrogen to form atomic hydrogen. Atomic hydrogen then diffuses into the metal oxide structure, rupturing the metal-oxygen bond. The rupture is caused by heterolytic hydrogen, which forms hydroxyl groups and metal hydride for

most metal oxides or H_2O with the bridging oxygen of the metal oxide, creating a vacancy [27]. The volatile metal hydrate will release the hydrate, forming water vapour, which will desorb, creating a reduced metal, ready for use. An overly simplified version of the reaction is illustrated in equation 2.4.

$$MO_x + xH_2(g) \rightarrow M + xH_2O(g) \tag{2.4}$$

Temperature-programmed reduction (TPR) is a common analysis method used to characterize the oxo-reductive properties of metal oxide catalysts. Using H_2 (or sometimes CO) as the reduction agent to reduce the solid sample during a set heating rate, and monitoring the flow rate using a mass spectrometer (MS) or thermal conductivity detector (TCD) makes it possible to characterize at which temperature the solid sample is reduced [28]. In engineering, TPR is used to determine the optimal reduction conditions for a broad range of metal oxides used in catalytic reductive reactions [28].

2.4.4 Diffuse Reflectance Infrared Fourier Transform Spectroscopy

Shining light through any type of absorptive medium results in the absorption of specific wavelengths, causing a change in perceived light. One common natural phenomenon observed every day is that of chlorophyll, the substance responsible for transforming sunlight into energy in plants. Chlorophyll is exceptionally good at absorbing sunlight from most visible wavelengths except those between approximately 500-550 nm, which corresponds to the green colour.

The absorbance of light of any absorbing medium is characterised by the Beer-Lambert equation, shown in Equation 2.5, where the resulting intensity I, of any given wavelength, is dependent on incident intensity I_0, the length of the path through the absorbing medium x, and the absorption coefficient k, which is an entire function depending on the wavelength of light absorbed [29].

$$I = I_0 \cdot e^{-k \cdot x} \tag{2.5}$$

In the case of DRIFTs, the absorbed energy of light creates characteristic vibrational frequencies of molecular bonds as a way to release excess energy. DRIFTs is used to analyse molecular composition in terms of molecular bonds and vibration frequencies using probe molecules such

as CO or CO_2 to determine key characteristics of powders and/or polymers [29]. The probe molecules adsorb to the active sites on the catalyst surface, whereas analysis can be performed to characterize the properties.

3

Methods

To answer our questions whether hydrogenative catalytic depolymerisation of nylon 6 using acid base properties of catalyst supports might be a valid solution to improve catalytic recycling depolymerisation methods, and if the acid-basic properties of Ru/ZrO_2 based metal-oxide catalysts has an effect on the conversion of nylon-6 to ϵ-caprolactam, a series of tests were performed to determine the effectiveness of the Ru/ZrO_2 based catalyst. Developed to fit the requirements of the work, the work was divided into three main parts: catalyst sample preparation, characterizing the catalysts, and activity tests, including reaction product quantifications.

The catalyst preparations involved the synthesis of the supports and the impregnation of the active ruthenium metal, while the characterization of the supports was carried out using analysis methods including: X-Ray Diffraction (XRD); Hydrogen Temperature Programmed Reduction (H_2-TPR); Ammonia- and carbon dioxide Temperature Programmed Desorption (NH_3-TPD and CO_2-TPD); as well as nitrogen physisorption. The reaction tests were then performed to investigate the properties and their effect on catalytic depolymerisation.

3.1 Synthesis of zirconia based metal oxide catalysts

The zirconia-based metal oxide catalysts were synthesized using the co-precipitation method, which was carried out by dissolving MgO ($Mg(NO_3)_2 \cdot 6H_2O$, 99%, bought from Sigma Aldrich), SrO ($Sr(NO_3)_2$, 100%, bought from Sigma Aldrich), WO_3 ($(NH_4)_6H_2W_{12}O_{40} \cdot xH_2O$, 92%, bought from Fluka Analytics), Y_2O_3 ($Y(NO_3)_3 \cdot 6H_2O$, 99,8%, bought from Sigma Aldrich), or La_2O_3 ($La(NO_3)_3.6H_2O$, 100%, bought from Fluka Analytical) precursor solutions, corresponding to 10 wt% metal oxide (MgO, SrO, WO_3, Y_2O_3 or La_2O_3), together with zirconia precursors in 300 ml of distilled water. The amounts of samples prepared were such that the final amount of MO_x-ZrO_2 support was approximately 12-13 grams, enough to perform all

the required characterization and activity measurements and still have some support left in case later needed for similar co-precipitated catalysts or in case something went wrong. In this study, zirconyl nitrate hydrate ($ZrO(NO_3)_2.xH_2O$, 99,5%, Thermo Scientific) was used as a result of its simplified synthesis steps and ease of handling. Precursors such as zirconyl chloride require stricter handling and disposal, as well as a more difficult separation process to avoid catalyst poisoning [30], motivating the use of nitrate precursors instead.

For the first couple of batches, ethanol, expected to provide smaller particles and a narrow particle size distribution, was used in a 1:1 ratio with water, but was quickly deemed unnecessary after physisorption measurements and that the precursor was still fully dissolved without ethanol. The solvent was subsequently switched to pure distilled Milli-Q water. A preliminary study on the use of polyethylene glycol (PEG) was also performed to test whether PEG would work as a stabilizer. By theoretical assumptions, PEG would form the template for the support structure, which, when calcined, would burn off, forming the desired porous catalyst structure. This method was discontinued when the results of the N_2 physisorption measurements did not show significant improvements in SSA in contradiction to the previous hypothesis. For PEG-stabilized ZrO_2, the measured SSA was 41,9 $\frac{m^2}{g}$ compared to the nearly 50 $\frac{m^2}{g}$ obtained by La-stabilized ZrO_2 and pure ZrO_2 according to previous studies at the department.

Following dissolution of the support precursors, the support was precipitated using an ammonia hydroxide (NH_4-OH) solution to a pH of 9; This was done with approximately 10-15 ml of NH_4OH for the 300 ml water solution. Increasing the pH of the solution to 9 was expected to fully precipitate the co-precipitated support. Following precipitation of the solution, the solution was aged for 18 h at 80 °C under reflux conditions. Subsequently, the solution was filtered, dried at 100°C, and mortared to allow a fine powder to be prepared for calcination. Calcination was carried out in a furnace, with a heating rate of 2°C/min, up to 700°C, held for 5 h, then naturally cooled at ambient temperatures. After calcination, the support structure was finished and ready to form the active catalyst particle after the metal was added.

3.1.1 Commercial ZrO_2-based catalysts

Based on the N_2 studies and reaction tests of the co-precipitated catalysts, supports similar to the co-precipitated support-catalysts were synthesized by incipient wetness impregnation (IWI) of the metal oxide precursor solution of MgO, SrO and WO_3 on a pre-calcined commercially

available ZrO_2 support (UEP-100, available from DAIICHI KIGENSO KAGAKU KOGYO CO., LTD). The drying and calcination of the supports to remove residual precursor nitrates was carried out the same way as for the co-precipitated ZrO_2-based catalysts, except that the calcination of the commercial MO_x-ZrO_2 supports were done at 500°C instead of 700°C.

3.1.2 Active metal loading of Ruthenium

With the supports prepared, the active metal loading of ruthenium was performed using IWI to prepare the catalysts for depolymerisation tests. The precursor solution used was Ruthenium (III) nitrosyl nitrate, with the chemical formula $Ru(NO_3)_3NO$. The counterion $[(NO_3)_3NO]^{3-}$, was easily removed during calcination. The calcination following the impregnation of ruthenium was carried out at a heating rate of 2°C/min up to 500°C for the co-precipitated catalysts, while at 400°C for the commercial ZrO_2 based catalysts. The temperature was then maintained for 5 h and then naturally cooled down. The amount of precursor solution added was determined by N_2 physisorption measurements of the supports to be equal to the pore volume. The amount of prepared catalyst was determined to be 3 grams of finished Ru-MO_x-ZrO_2 catalyst. The active metal loading used was 1 wt% of the total weight, in this case 0,03 g of ruthenium for 2,97 g of MO_x-ZrO_2 support. This number was determined based on previous studies conducted at the department [9].

3.2 Catalyst characterisation

To understand the relationship between the properties of the depolymerisation catalyst, several analysis methods were used. These are used to relate the properties of the catalyst to the catalytic activity, a measure of the catalytic efficiency. Of the several analysis methods presented previously, XRD was used to characterize the phase of the catalyst, while H_2-TPR, CO_2-DRIFTS were used in order to provide data on the metal-support interactions and the reducibility of the catalyst. N_2 physisorption was used mainly to identify surface morphology properties, while NH_3-TPD and CO_2-TPD were used in conjunction to measure the nature and properties of acidic and basic sites. N_2 physisorption was also used to characterize the morphology of the catalyst by measuring the pore volume, diameter, and surface area. ICP-MS was also used to characterize the wt% of the metal loading on the finished catalysts.

3.2.1 N_2 physisorption

Measurement of textural properties, such as pore volume, pore diameter, and specific surface area, was performed on a Micromeretics Tristar 3000 instrument. Before measurements, the samples were degassed in nitrogen at 200°C, for 5 h. The measurements were then taken under liquid nitrogen conditions to maintain a temperature of -196°C. The total surface area was calculated using the BET equation as described in Equation 2.1, while the pore diameter and pore volume were obtained using the BJH equation.

3.2.2 X-Ray Diffraction (XRD)

XRD patterns were obtained by performing analysis using the Bruker D8 Discover instrument with a CuKα (λ = 1,54 Å) radiation source, available at the Chalmers Materials Analysis Laboratory (CMAL), with 2θ increments of 0,04°, scanning between 2θ = 10-70°. The diffractogram was then compared using online databases, matching the diffractogram with the known database of crystallographic structures and planes to identify the crystal structure and unit cell parameters.

3.2.3 Diffuse Reflectance Infrared Fourier Transform Spectroscopy

Diffuse Reflectance Infrared Fourier Transform Spectroscopy (DRIFTS) was used to investigate the acid base properties and chemisorption strengths of CO for the catalyst samples by FT-IR methods. The spectra were obtained using a Vertex 70 instrument by Bruker equipped with a diffuse reflectance accessory, as well as a coupled mass spectrometer to analyse the nature of adsorbed and desorbed species of the gas flow coming out of the sample chamber.

The DRIFT measurements were performed according to a set schedule. In general, the steps include a pretreatment using 8000 ppm H_2 while heating to 250°C and then cooling to 35°C. The background measurements were then taken at 35°C, and thereafter the measurement began. This was done by introducing 1000 ppm CO for 1 h at 35°C. After flushing the system with Ar, the final spectra were recorded.

CO_2-DRIFTs was done similarly with the same pretreatment, and a background measurement was taken at 35°C. The sample was then introduced to 1000 ppm CO_2 at 150°C for 30 min

followed by flushing with Ar for 30 min to remove any weakly bonded CO_2. The DRIFT spectra was then recorded at 35°C.

To measure the weaker adsorption sites, adsorption of CO_2 was also done at 35°C for 30 min, followed by 30 min of Ar to flush the system. The difference between the total and stronger adsorption measurements gave the weaker adsorption sites.

3.2.4 Temperature Programmed Desorption (TPD)

Temperature-programmed desorption (TPD) measurements using CO_2 and NH_3 were performed on a calorimeter (Sensys DSC, SETARAM) coupled with a HPR-20 QUI mass spectrometer. TPD measurements were used to investigate the basic and acidic properties respectfully of the catalyst samples.

The CO_2-TPD measurements were performed by pretreatment of $\approx$ 40-60 mg of sample under an atmosphere of Argon at 200 °C for 20 min. 8000 ppm H_2 gas (3,5% H_2/Ar) was then introduced at 200°C for 20 min and then heated to 250°C at a rate of 10°C/min to match the reduction condition of the activity tests. H_2 flows for 10 min, after which the system is flushed with Ar for 20 min. The temperature was then increased to 300°C and held for another 30 min to remove all H_2. The pretreatment was then completed with the cooling of the sample tube to 40°C.

After pretreatment, 5000 ppm of CO_2 (2% CO_2/Ar) was then introduced for 2 h then flushed with Ar at the same temperature (40°C) for 1 h. The sample was then heated at 10°C/min from 40-700°C with continuous Ar flow, then kept at 700°C for 30 min to induce CO_2 desorption. The desorption of CO_2 was tracked during desorption using a mass spectrometer set to monitor several gases, one of which being CO_2, at a mass number m/z = 44.

NH_3-TPD was conducted similarly to the CO_2-TPD measurements with the same pretreatment and similar measurement. After pretreatment, the sample was cooled to 100°C and 2000 ppm NH_3 was introduced for 2 h, then flushed with Ar for 1 h at the same temperature to remove any loosely adsorbed NH_3. The desorption measurements were then started by heating 100-700°C at a rate of 10°/min while monitoring NH_3 using a mass spectrometer, at the mass number m/z = 17.

3.2.5 Temperature Programmed Reduction

The temperature-programmed reduction of the catalysts was performed using hydrogen (H_2-TPR) using the same calorimetric instrument as for the TPD measurements, with a total flow of 20 ml/min during the procedure.

The measurements began with a pretreatment with argon at 300 °C for 30 min, following a flush of the sample with 8000 ppm hydrogen (3,5% H_2/Ar) for 20 min at 25°C. After pretreatment, the sample was heated from 25-800°C under H_2 flow at a rate of 10°C/min, and held at 800°C for another 30 min. During this process, hydrogen flow was tracked using the mass spectrometer set up to monitor H_2 at the mass number m/z = 2.

3.3 Catalytic activity

To relate the characteristics with performance and efficiency, a series of experimental tests of catalyst activity are required. As a preparation, commercially purchased nylon-6 was ground into smaller particles <0.5 mm using cryo-grinding methods to be used during the depolymerisation of nylon-6 reaction tests.

Based on a previous study [9], activity measurements were performed in a 450 ml Parr batch reactor in an atmosphere of $\approx$ 300°C and 30 bars of H_2. The following presents a general description of the method. Prior to activity measurements, the catalyst was reduced. This was done by pressurizing the reaction vessel with 10 bars of H_2, heating at a rate of 10°C/min to 250°C, and then holding the temperature for 2 h. Before activity tests are performed, the reaction vessel was loaded with catalyst, nylon-6 and solvent, in this case about 75 ml of hexadecane, each of which noted the actual weights of the components added, flushed with nitrogen for some cycles, and pressurized to 30 bar H_2. After pressurization, the reactor was heated at a rate of 10°C/min to 300°C and held for 2 h. The reaction setup is illustrated in Figure 3.1.

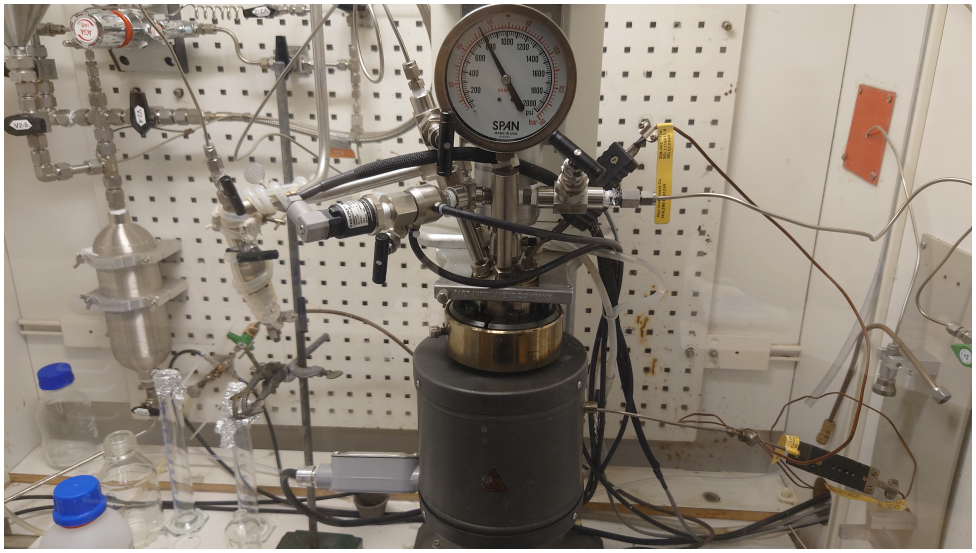

Figure 3.1: The activity test of a catalyst performed in a Parr 450 ml batch reactor

After the reaction, the reactor was quenched with cooling water at ambient temperatures, vented to atmospheric pressure, and purged by nitrogen. The products of the reaction were subsequently analysed using GC-MS/FID and DSC.

Gas-chromatography coupled with an mass spectrometer (GC-MS) that detects and identifies molecular fractions and their respective masses was used to quantify the amount of ϵ-caprolactam obtained from the reactor by identification based on retention times obtained by the GC instrument. For the Hexadecane samples, the GC was run with an oven set at 280 °C to quickly vaporize the solvent and sample entering the column. The inlet of the column was set at 1,78 bar and a total throughput of 2 ml/min, including He carrier gas, was used through the column based on a 50:1 methanol to sample split. The ethanol samples were performed similarly, with 280 °C, 0,87 bar at the input, 0,7 ml/min throughput, and a split flow of 100:1. During the study, MS was used predominantly to quantify ϵ -caprolactam concentrations by comparing the peak area ratio of ϵ-caprolactam/internal standard (CL/IS) obtained by the GC-MS instrument and to compare with standards previously run with known concentrations of ϵ-caprolactam corresponding to the CL/IS ratio. Using the obtained information, the effectiveness of each catalyst reaction was quantified by measures of conversion, yield, and selectiveness.

4

Results and Discussion

To test whether properties such as the presence of acidic and basic sites and the structure of the metal oxide composite material affect the properties of the catalyst, numerous samples were prepared. The samples prepared and studied during the work are summarized in Table 4.1, where the expected metal loading is shown in the catalyst name, where $10MO_x$ indicates an expected metal oxide loading of 10 wt% of the support. The actual metal oxide compositions of several catalyst samples used for depolymerisation reaction tests were obtained by ex situ Induced Coupled Plasma Mass Spectroscopy (ICP-MS), performed by ALS Scadinavia AB Luleå and shown in the columns to the right in Table 4.1, but due to the limitation of the ICP-MS method of dissolving Ru with acid as part of the sample preparation, the expected 1 wt% Ru loading could not be accurately quantified using ICP-MS.

The first two samples of ZrO_2 were prepared identically except for the fact that they were synthesized using two batches of zirconyl nitrate hydrate. This was done because the first batch did not fully dissolve in the water/ethanol solution and was hypothesized to be due to contaminations as a result of previous uses and storage under ambient conditions. The La_2O_3-10SrO-ZrO_2 catalyst, as shown last under "Co-precipitated catalysts" in Table 4.1, was synthesized by co-precipitation but calcined at 500 °C to investigate the effect of lower calcination temperatures.

Table 4.1: All catalysts prepared during the study, including expected and actual metal loadings.

Sample	La_2O_3	MgO	SrO	WO_3	Y_2O_3	Mn
Co-precipitated catalysts, 700°C Calcination						
ZrO_2-a*/**	-	-	-	-	-	-
ZrO_2-b*/**	-	-	-	-	-	-
Ru/2Y_2O_3-ZrO_2**	-	-	-	-	0,5	-
10Y_2O_3-ZrO_2**	-	-	-	-	-	-
Ru/6La_2O_3-ZrO_2	5,4	-	-	-	-	-
Ru/6La_2O_3-10MgO-ZrO_2	6,0	2,9	-	-	-	-
Ru/6La_2O_3-10MgO(IWI)-ZrO_2	4,5	9,4	-	-	-	-
Ru/6La_2O_3-10SrO-ZrO_2	6,4	-	2,2	-	-	-
Ru/6La_2O_3-10WO_3-ZrO_2	5,5	-	-	8,2	-	-
La_2O_3-10SrO-ZrO_2***	-	-	-	-	-	-
Commercial ZrO_2 catalysts, 500°C Calcination						
Ru/10SrO-ZrO_2	-	-	9,7	-	-	-
Ru/5SrO-ZrO_2	-	-	5,6	-	-	-
Ru/1SrO-ZrO_2	-	-	1,0	-	-	-
Ru/10WO_3-ZrO_2	-	-	-	8,6	-	-
Ru/10MgO-ZrO_2	-	-	-	9,2	-	-
Ru/7WO_3-3SrO-ZrO_2	-	-	3,0	7,0	-	-
Ru/0,5Mn-ZrO_2	-	-	-	-	-	0,8
Ru/ZrO_2	-	-	-	-	-	-

* Samples prepared from two different batches of zyrconyl nitrate hydrate.

** Samples were prepared but due to undesired properties were excluded as part of reaction testing.

*** Sample was prepared by co-precipitation but calcined at 500°C.

Of the numerous samples, those prepared by ruthenium impregnation were mainly determined by the expected acid-basic characteristics of the supports. Some samples were planned for depolymerisation tests, such as the Ru/2Y_2O_3-ZrO_2 and Ru/6La_2O_3-ZrO_2, but were excluded due to time constraints and the general trend of low conversion from similar co-precipitated catalysts.

The co-precipitated, basic catalyst supports with MgO and SrO loading showed a lower than expected metal loading, likely due to an incomplete understanding of the precipitation conditions of the metal oxide precursors.

4.1 Powder X-ray Diffraction

The samples were analysed using (XRD) to characterize the crystallographic structure of the samples. The structure and Miller indices of each ruthenium-impregnated sample were determined by matching the diffractogram to the PDF 5+ database (Powder Diffraction File) maintained by the Internation Center for Diffraction Data (ICDD), previously JCPDS, and the previous literature.

4.1.1 Co-precipitated La_2O_3-ZrO_2-based catalysts

From the several samples analysed, the diffractogram of the co-precipitated catalysts Ru/MgO-La_2O_3-ZrO_2, Ru/SrO-La_2O_3-ZrO_2, Ru/WO_3-La_2O_3-ZrO_2 and Ru/La_2O_3-ZrO_2 showed no signs of MO_x crystals, and the 2θ = 30,2; 35,2; 50,6; 60,0 and 60,5 matched the ZrO_2 cubic phase (JCPDS 88-1007) [31], as illustrated in Figure 4.1, indicating negligent effects from the incorporated metal oxide on crystal structure of the catalysts. This also shows the ZrO_2 phase change of La_2O_3 incorporated into ZrO_2-based supports to form the cubic phase. These samples did not show discernible differences, except for a small peak at $2\theta = 28$, probably as a result of the incorporated metal oxides.

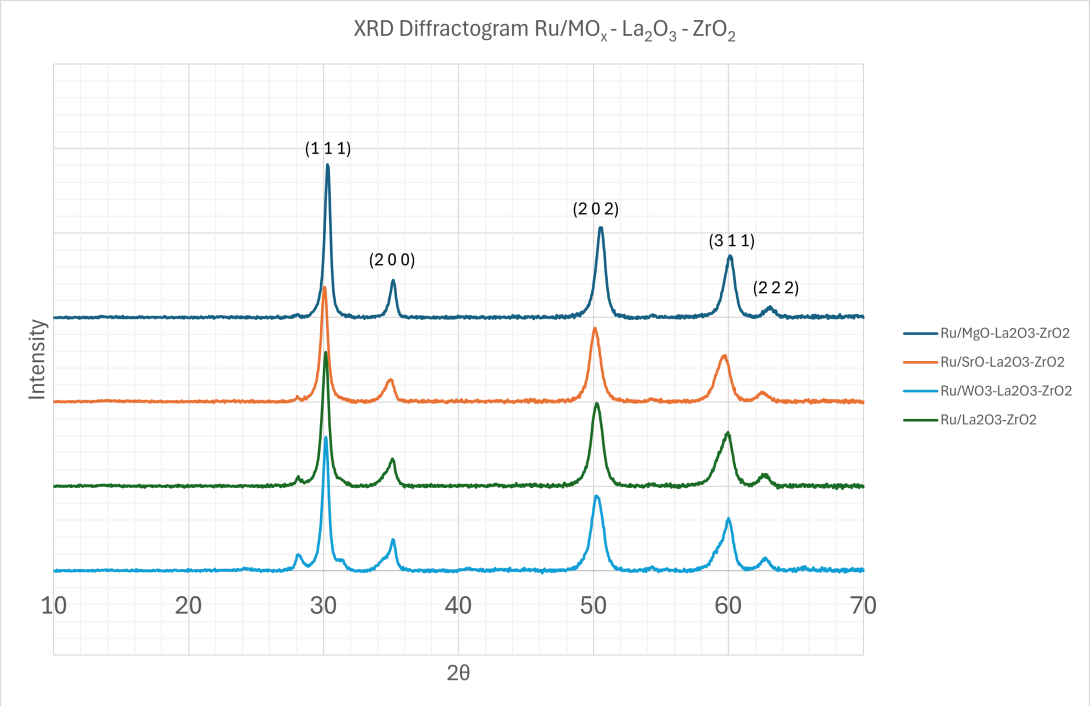

Figure 4.1: Diffractogram obtained from the sampling of ZrO_2-based metal oxide composites, calcined at 700°C, with La_2O_3 as a stabilization agent. The crystallographic structure, as indicated by Miller indices, strongly indicate a stabilised cubic phase.

4.1.1.1 Yttrium Stabilized Zirconia diffractogram

The diffractogram from YSZ was also studied to determine the characteristics of one such catalyst. The XRD diffractogram with the main peaks at 2θ = 28,2; 31,5; 34,3; 35,3; 49,3; 50,1 and 55,5, illustrated in Figure 4.2 shows an almost exclusive monoclinic ZrO_2 phase (ICDD #00-037-1484) as compared to the samples illustrated in Figure 4.1.

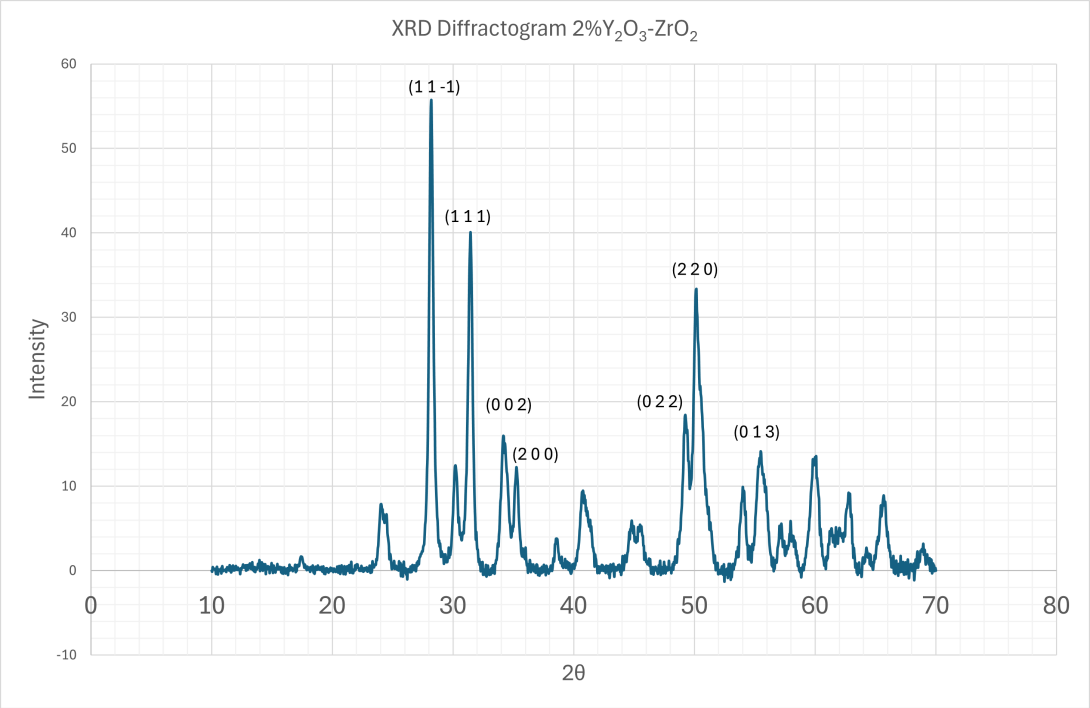

Figure 4.2: Diffractogram from 2 weight% YSZ with matching crystallographic planes indicated by Miller indices, highly indicating a monoclinic phase.

4.1.2 Commercial ZrO_2-based catalysts

XRD was also performed on the commercial ZrO_2-based catalyst. The diffractogram of the Ru/MO_x-ZrO_2 catalysts, as shown in Figure 4.3, shows a monoclinic zirconia phase (ICDD #00-037-1484), almost identical to those of the YSZ catalysts, with the same crystallographic planes as those of the YSZ catalyst. An extra peak can be identified from the diffractogram of the Ru/10MgO-ZrO_2 catalyst at $2\theta \approx 43°$. This is likely to be seen due to the formation of a different kind of Mg-Zr phase; however, the overlap with the monoclinic ZrO_2 phase or the lack of any other discernible peaks makes it difficult to identify or quantify.

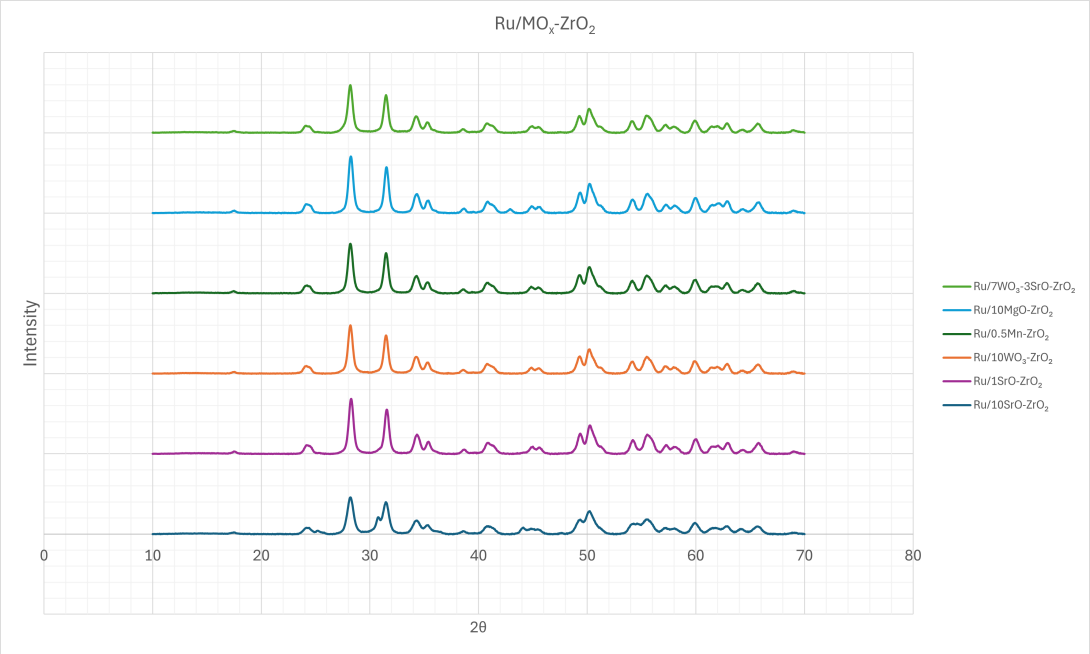

Figure 4.3: Diffractogram of commercial ZrO_2-based catalysts, showing mainly monoclinic phase ZrO_2.

As can be seen in Figure 4.3, there is a slight difference between the diffractograms of the Ru/SrO-ZrO_2 catalysts. These differences have been highlighted in Figure 4.4, isolating the plots and highlighting the individual peaks that differ between the two samples. The 10 wt% loaded Ru/10SrO-ZrO_2 catalyst shows a broad range of shoulders and peaks at 2θ = 25,2; 31,1; 34,9; 44,2; 49,6 and 54,9. These peaks are consistent with the $SrZrO_3$ phase (JCPDS 75-0467) [31], formed as a result of a higher SrO loading [31]. This shows that the loading of SrO causes a new phase to form alongside the monoclinic ZrO_2 phase. This new phase is an orthorhombic perovskite structure belonging to the Pnma/Pbnm (62) space group (in the International Tables for Crystallography) [32].

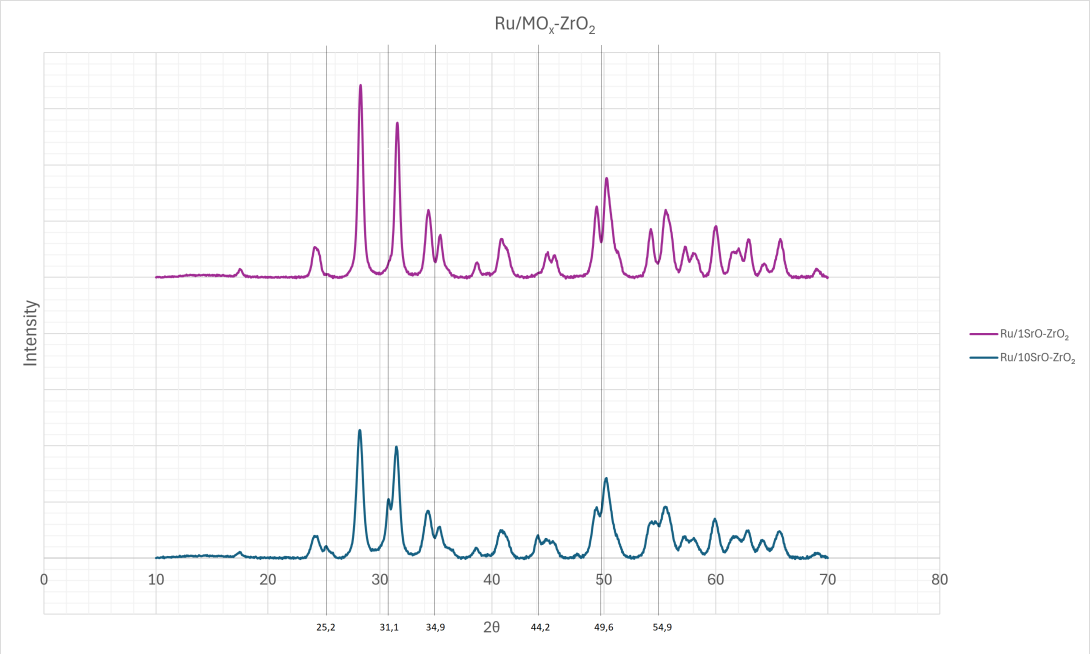

Figure 4.4: XRD diffractograms of Ru/SrO-ZrO_2 catalysts with 10 wt % and 1 % SrO loading. The extra peaks noticed in the Ru/10SrO-ZrO_2 catalyst indicated a $SrZrO_3$ perovskite structure.

4.2 N_2 Physisorption

The samples were also analysed using N_2 physisorption measurement techniques to obtain the pore volume, diameter, and specific surface area, while the total pore volume was used to calculate the impregnation volume for the incipient wetness impregnation of the Ru- and MO_x precursors.

The results, which are summarized in Table 4.2, showed relatively small differences in surface areas for most co-precipitated catalysts, except for the YSZ supports, showing an almost 50% decrease in SSA (22,2 $\frac{m^2}{g}$) and more than double the average pore diameter (14,3 nm vs 7-9 nm average) for the 2 wt% Y_2O_3-ZrO_2 support while maintaining non-discernible average pore diameter (6,7 nm) for the 10 wt%Y_2O_3-ZrO_2 support as compared to the other La_2O_3 stabilized supports. This is likely also due to the different crystalline phases of the YSZ supports, showing a mainly monoclinic phase, while the other lanthanum-stabilized zirconia (LSZ) supports showed a cubic phase, indicating the lower stability of the YSZ supports (monoclinic ZrO_2) calcined at 700 °C.

Similarly to the YSZ supports, both the co-precipitated Ru/La_2O_3-10MgO-ZrO_2 and commer-

cial ZrO_2-based Ru/10MgO-ZrO_2 catalysts showed a similar decrease in SSA of almost 50% (29,2 and 28,8 $\frac{m^2}{g}$), as compared to the standard La_2O_3-ZrO_2 support (51,7 $\frac{m^2}{g}$) and Ru/ZrO_2 (70,1 $\frac{m^2}{g}$) catalyst. This is likely due to the blocking of smaller pores as a result of the smaller atomic radii (150 pm) of the Mg atom compared to the larger Sr (219 pm), W (193 pm) or La (226 pm) [33], which is also supported by the smaller pore volume ($\approx 20\%$ less) and the larger average pore diameter ($\approx 30\%$ larger), when compared to the La_2O_3-ZrO_2 support. The La_2O_3-10SrO-ZrO_2 support, as shown last in the Co-precipitated catalysts list in Table 4.2, was synthesized from the calcination at 500 °C of the same support used for the Ru/La_2O_3-10SrO-ZrO_2 catalyst, was excluded from further testing due to the low pore diameter (3,1 nm vs 6,7 nm for Ru/La_2O_3) as characterized by N_2 physisorption.

Table 4.2: Physisorption measurements of catalytic particles including surface area, pore volume and average pore diameter.

Sample	**Surface Area** $\frac{m^2}{g}$	**Pore Volume** $\frac{cm^3}{g}$	**Pore Diameter** (nm) (Average)
Co-precipitated catalysts, 700°C Calcination / 500°C Ru Calcination			
ZrO_2-a*	41,9	0,18	15,1
ZrO_2-b*	52,9	0,15	9,6
10%Y_2O_3-$Zr0_2$	25,2	0,05	6,7
Ru/2%Y_2O_3-$Zr0_2$	22,2	0,10	14,3
La_2O_3-ZrO_2	51,7	0,10	6,5
Ru/La_2O_3-ZrO_2	49,4	0,10	6,7
Ru/La_2O_3-10MgO-ZrO_2	29,2	0,08	8,7
Ru/La_2O_3-10MgO(IWI)-ZrO_2	25,9	0,06	7,8
Ru/La_2O_3-10SrO-ZrO_2	40,6	0,08	6,6
Ru/La_2O_3-10WO_3-ZrO_2	43,1	0,11	8,3
La_2O_3-10SrO-ZrO_2**	107,2	0,10	3,1
Commercial ZrO_2 catalysts, 500°C Calcination / 400°C Ru Calcination			
Ru/10SrO-ZrO_2	52,8	0,25	16,2
Ru/5SrO-ZrO_2	60,2	0,27	14,8
Ru/1SrO-ZrO_2	45,6	0,18	13,7
Ru/10WO_3-ZrO_2	42,3	0,17	14,5
Ru/10MgO-ZrO_2	28,8	0,18	18,7
Ru/7WO_3-3SrO-ZrO_2	41,4	0,18	14,8
Ru/0,5Mn-ZrO_2	43,5	0,21	16,1
Ru/ZrO_2	70,1	0,29	13,9

* Samples prepared from two different batches of zyrconyl nitrate hydrate.

** Sample was prepared by co-precipitation but calcined at 500°C.

As a reference, the La_2O_3-10SrO-ZrO_2 was also prepared but calcined at 500°C to investigate the effect of lower calcination temperatures of the lanthanum-stabilized zirconia catalyst supports. However, after N_2 physisorption measurements, the relatively low pore diameter of 3 nm,

compared to the catalyst samples prepared by co-precipitation, averaging 7-9 nm, caused the sample to be discarded for further testing. A standard Ru/La_2O_3-ZrO_2 catalyst was also synthesized but with impregnated rather than co-precipitated MgO as a response to the relatively low surface area of Ru/MgO-La_2O_3-ZrO_2, as shown in Table 4.2.

In the second part of the study, where the metal oxides impregnated on commercially bough ZrO_2 were used instead, there were clear differences in SSA ($\approx 14 - 40\%$ decrease) and pore volume ($\approx 10 - 41\%$ decrease) between the Ru/MO_x-ZrO_x and Ru/ZrO_2 catalysts, while the average diameter of the pores only increased slightly.

4.2.1 Isotherms

The isotherms of the physisorption measurements were also analysed to determine the pore structure of the catalysts during the study. The results showed that the pore structure was mainly dependent on the preparation method, where the isotherm shape barely differed between different co-precipitated or commercial ZrO_2 catalysts. The difference is shown in Figure 4.5 and illustrates the general difference between the pore structure of the catalysts. Commercial ZrO_2-based catalysts showed a type III adsorption isotherm based on the IUPAC classification, indicating a macroporous structure [34]. However, the co-precipitated catalysts showed a type IV adsorption isotherm with a hysteresis loop according to the H_4 classification, indicating a mesoporous structure, with narrow slit-shaped pores [34].

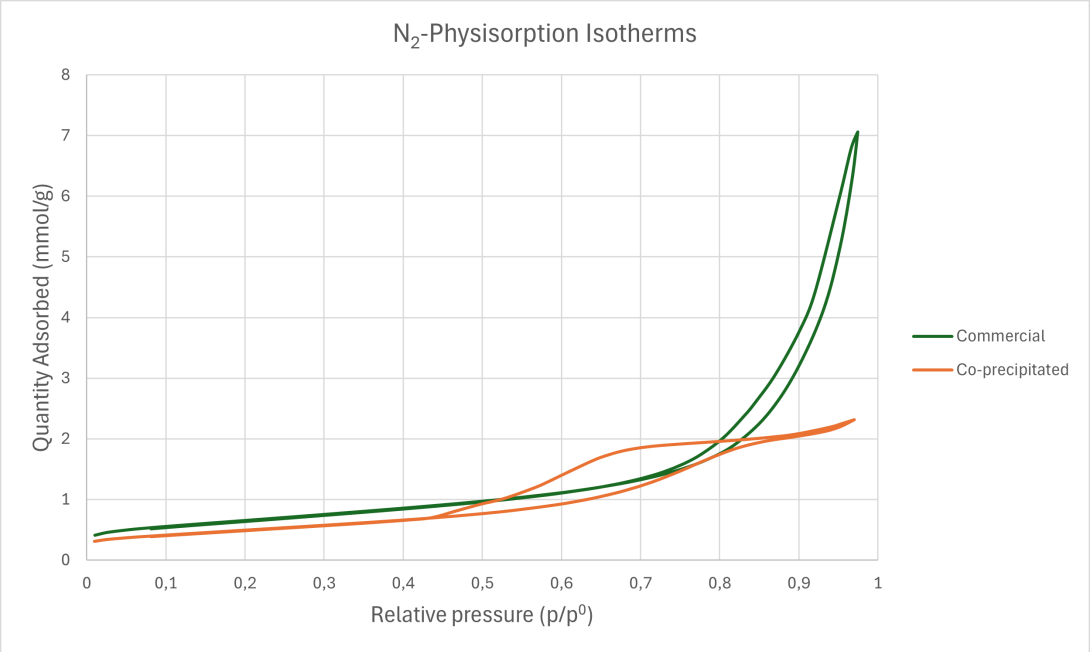

Figure 4.5: Representative shape of the physisorption isotherm between co-precipitated and commercial ZrO_2-based catalysts.

4.3 Temperature Programmed Reduction

Temperature programmed reductions (TPR) were performed to determine the reduction conditions of the catalyst samples as well as the difference in metal-support interactions between each sample, which causes shifts in peak positions. The results of the measurements showed many similarities between the different samples, where most of the reductions of ruthenium oxides occurred between 130-150 °C [35]. The H_2-TPR profiles for the main samples are represented in Figure 4.6.

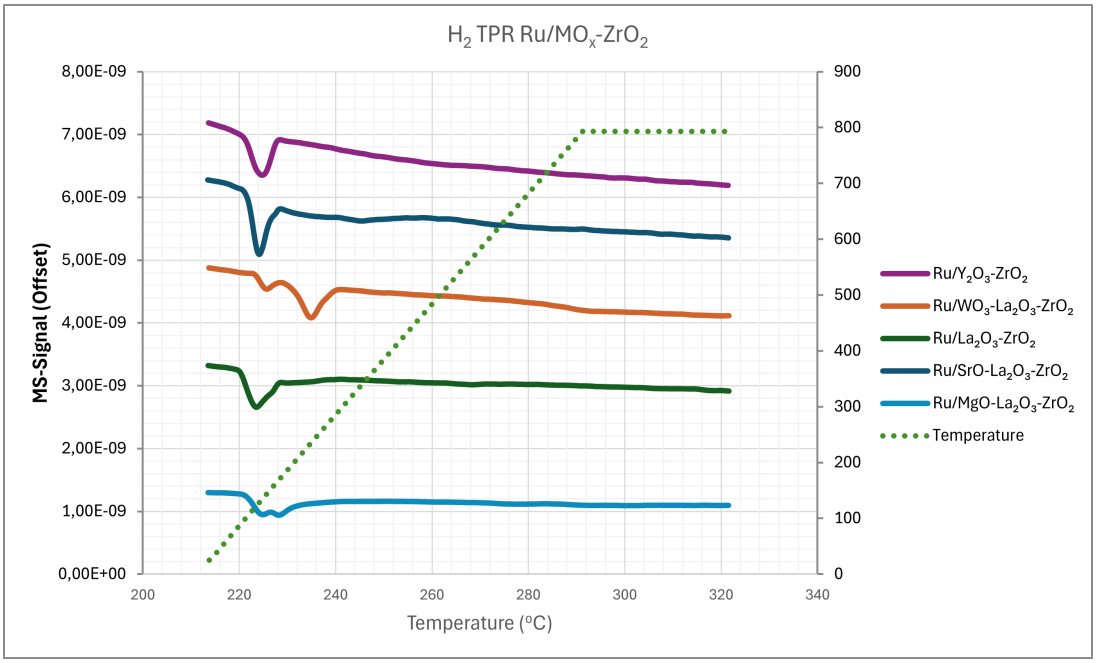

Figure 4.6: H_2-TPR profiles of co-precipitated catalysts. where most catalysts exhibit similar properties except the Ru/WO_3-La_2O_3-ZrO_2 catalyst, showing an extra reduction peak at 240 °C.

Each sample shows two main peaks in the 130-150 °C region, indicating two types of Ru reductions, probably as a result of Ru reductions when bonded to ZrO_2 or MO_x [35]. The different metal-support interactions cause differences in the reduction temperatures, shown in the reduction temperature profiles of each catalyst in Figure 4.6. The only difference in reduction temperatures compared to the other catalysts is shown by the Ru/WO_3-La_2-O_3-ZrO_2 catalyst, where a secondary reduction peak at 240 °C is shown, likely as a result of stronger Ru-WO_3 interactions or higher WO_3 wt% compared to other metal oxides.

4.3.1 Commercial ZrO_2-based catalysts

Commercial ZrO_2-based catalysts were also investigated by H_2-TPR. This showed a larger variety of reduction temperatures in comparison to those of the co-precipitated catalysts. The H_2-TPR graph, illustrated in Figure 4.7, shows a wider range of reduction temperatures, likely as a result of the impregnated metal oxides, causing multiple Ru-MO_x interactions compared to co-precipitated catalysts. In general, three main peaks were visible, one at 221 minutes, corresponding to a temperature of 91°C, another at 228 minutes, corresponding to 165°C, and a third located around 243 minutes, corresponding to 323°C. Slight shifts between samples also occur,

such as the shift between the peak of 323°C of the Ru / 10MgO-ZrO2 and the Ru / SrO-ZrO2 catalyst, likely indicating a Ruthenium metal bound harder to MgO than for the similar case of Ruthenium bound to SrO, causing higher reduction temperatures. The peak corresponding to 165°C also shows a significant change between the basic MgO, SrO-based catalysts, and the acidic WO_3-based catalyst, showing a change in the reduction temperatures. The acidic catalyst also showed a shift of $\approx$ 10°C higher, probably as a result of stronger ruthenium bonding to WO_3 or greater coverage of WO_3, indicating that mostly Ru-WO_3 are getting reduced.

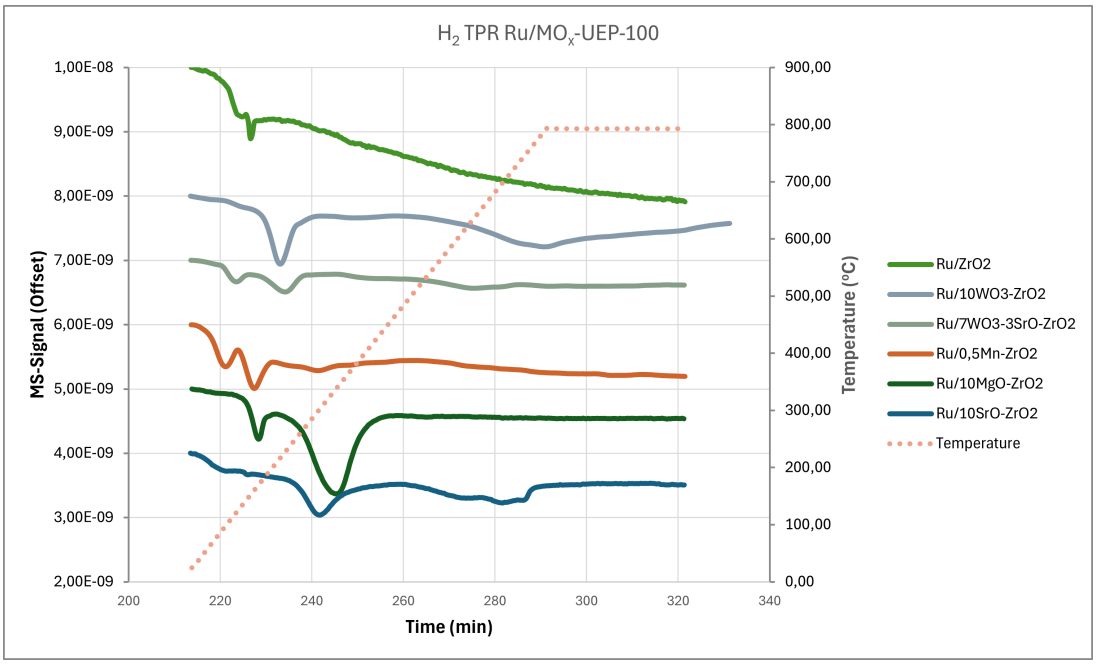

Figure 4.7: H_2-TPR of commercial zirconia catalyst samples

To try and explain the SrO loading of the Ru/SrO-ZrO_2 catalysts, a comparison of the TPR profiles was also performed to determine the effect of the loading on the reducibility and how it affects the catalytic efficiency. The results, shown in Figure 4.8, clearly show the difference in the SrO loading in the way ruthenium can be reduced. An increase in SrO loading increases H_2 consumption at 323 °C while decreasing the peak centred at 91 °C. This means that the increase in the SrO loading caused a change in Ru reduction, probably as a result of the increase in the Ru-SrO interactions.

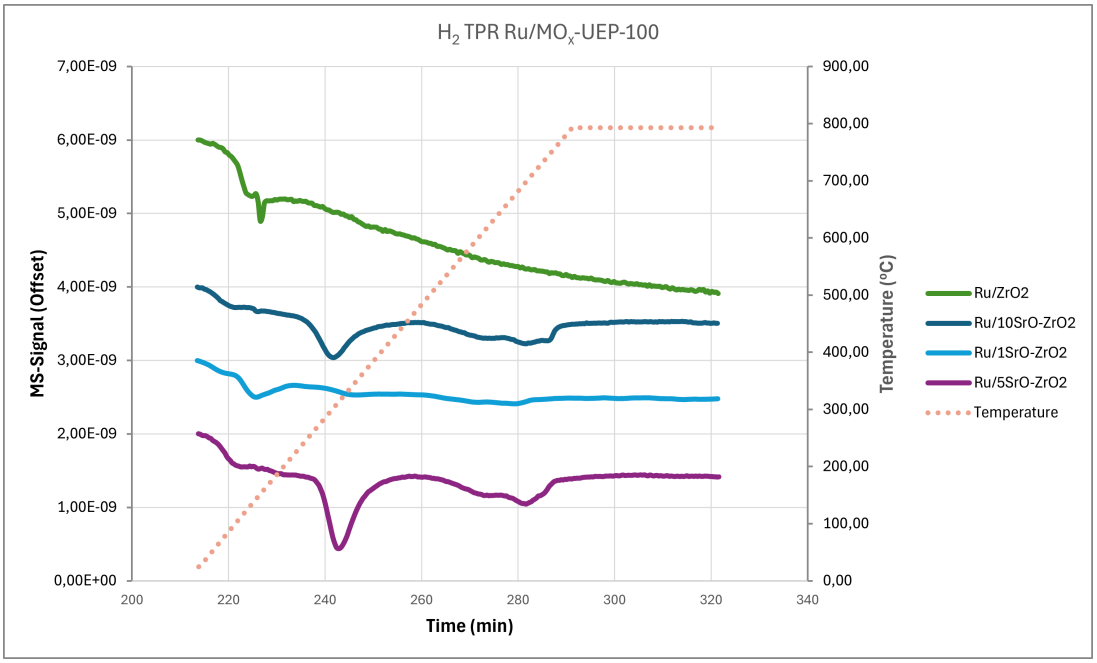

Figure 4.8: H_2-TPR of SrO-ZrO_2 based catalysts, showing the difference in reduction temperatures based of metal oxide support loading.

4.4 Temperature Programmed Desorption

TPD was used to investigate the basic acid properties of the catalytic sites present for each commercial ZrO_2 catalyst sample. The results, shown in Table 4.3, show a large difference between each sample in terms of basicity. The highest basicity is shown by the Ru/10SrO-ZrO_2 and Ru/5SrO-ZrO_2 catalysts, with respect to the desorption of 176 and 171 µmol/g CO_2 desorption respectfully. The highest acidity of the commercial ZrO_2 catalyst was shown to be the unmodified Ru/ZrO_2 catalyst, with 105,3 µmol/g NH_3 desorption. Compared to the 176,3 µmol/g CO_2 desorption as shown by the Ru/10SrO-ZrO_2 catalyst, none of the acidic catalysts tested increased the number of acidic sites, but instead decreased. This shows that the increase in acidic metal oxides by WO_3 incorporation did not increase the amount of acid sites, but rather covered or made inaccessible some of the sites, mainly by significantly altering acidic properties by WO_3-acidic site interactions, or forming a layer of WO_3, covering the acid sites.

Table 4.3: Desorption amount of CO_2/NH_3 as obtained by CO_2-TPD and NH_3 measurements.

Sample	CO_2 Desorption (µmol/g)	NH_3 Desorption (µmol/g)
Commercial ZrO_2 catalysts		
Ru/10SrO-ZrO_2	176,3	-
Ru/5SrO-ZrO_2	171,3	-
Ru/1SrO-ZrO_2	133,2	3,6
Ru/10MgO-ZrO_2	142,5	-
Ru/10WO_x-ZrO_2	-	39,2
Ru/7WO_3-3SrO-ZrO_2	81,7	4,1
Ru/0,5Mn-ZrO_2	102,9	-
Ru/ZrO_2	106,1	105,3

Only commercial zirconia catalysts were analysed due to the very low adsorption of CO_2 shown in the co-precipitated catalysts, which did not yield conclusive results. The CO_2 desorption graphs of the co-precipitated catalysts are shown in the Appendix A.1.

The CO_2-TPD for the most basic catalysts, being the SrO loaded and the Ru/ZrO_2 as a reference, as shown in Figure 4.9, showed 3 regions of CO_2-desorption. Weaker basic sites were prevalent at lower desorption temperatures of ≈160 °C, while medium and stronger adsorption sites were shown at ≈450 °C and 690 °C. A steady increase in stronger basic sites was observed with increased SrO loading. The weaker/medium basic site ratio of the Ru/SrO-ZrO_2 catalysts did not change much and was also present in the Ru/ZrO_2 catalyst, indicating that these basic sites are present mainly on the ZrO_2 metal oxide crystal structure and the SrO loading contributes to the strong basic sites.

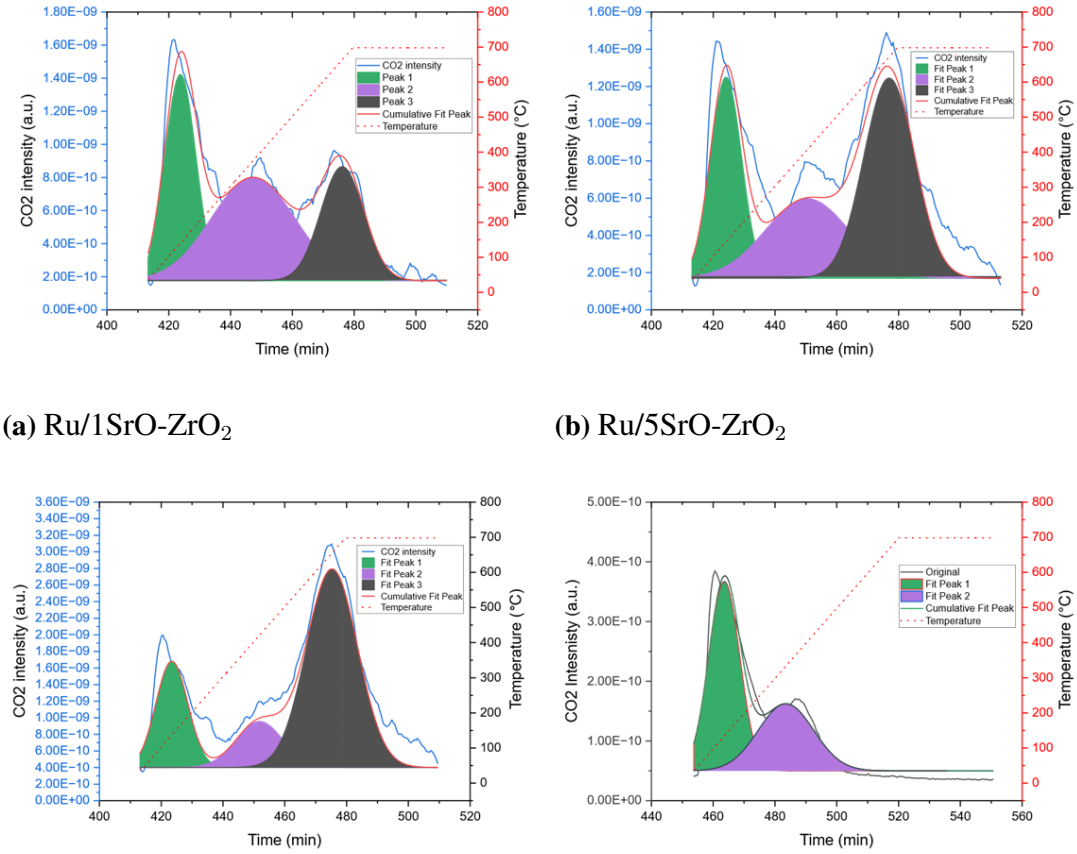

(a) Ru/1SrO-ZrO_2 **(b)** Ru/5SrO-ZrO_2

(c) Ru/10SrO-ZrO_2 **(d)** Ru/ZrO_2

Figure 4.9: CO_2-TPD with a fitted curve for the basic metal oxide catalysts. The increase in SrO loading of the Ru/SrO-ZrO_2 causes a steady increase in strong basic sites, while for the Ru/ZrO_2 catalyst, no strong basic sites are shown.

4.5 DRIFT

4.5.1 Co-precipitated ZrO_2-based catalysts

The CO-DRIFT spectrum of the Ru/MO_x-ZrO_2 co-precipitated catalysts, illustrated in Figure 4.10, showed several adsorption peaks between 1990 cm^{-1}, up to 2200 cm^{-1}, related to the vibrational frequencies of the molecular bonds present in the metal-carbonyl complexes. The strongest peak, attributed to the 2057 cm^{-1} wavenumber, can be ascribed to the C-O stretching vibration of the dicarbonyl CO species ($Ru^{n+}(CO)_2$) adsorption on single atomically dispersed Ru^{n+} sites [36]. The second largest peak, corresponding to the peak centred at 1990 cm^{-1} corresponds to the CO adsorbed on oxygen vacancies or Ru-doped ZrO_2 [36]. In between these

two is a smaller and less recognizable peak, blending in between the others, centred at about 2020 cm^{-1}, which can be attributed to the CO vibration of CO-linearly bound Ru sites with high coordination [36]. The two minor peaks, related to 2120 cm^{-1} and 2170 cm^{-1} can be ascribed to the rotational vibrational spectra of CO species of the gas phase [37][36]. The difference between the catalysts showed a large increase in Ru-CO vibrations for the $Ru/2Y_2O_3$-ZrO_2 catalyst compared to the other co-precipitated catalysts.

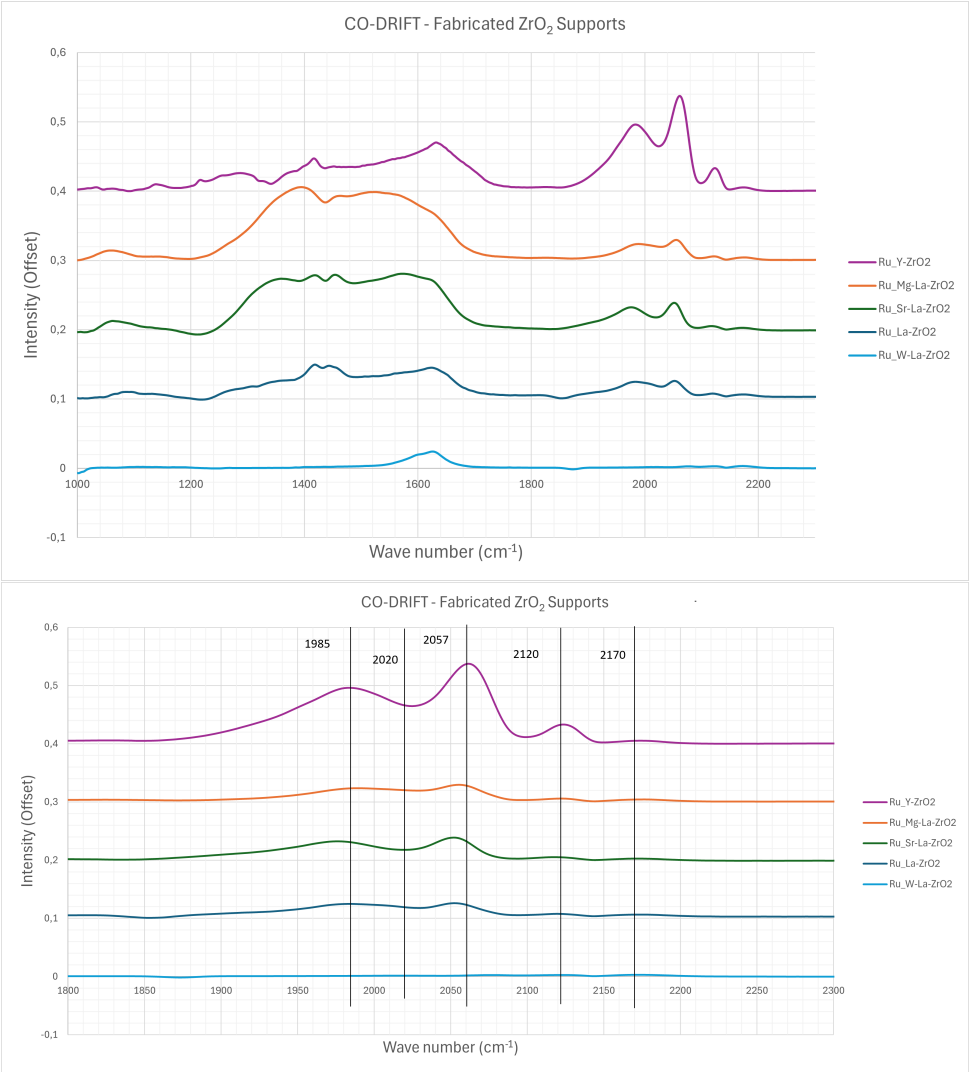

Figure 4.10: FT-IR Spectra of CO-DRIFT measurements taken for a select amount of co-precipitated Ru/ZrO_2 catalysts (top) as well as a zoom in on the Metal-ZrO_2 wavenumber ranges of 1800-2200 (bottom).

Another region, which was attributed to the vibrational wavenumbers of carbonate species, was visible from 1200-1700 cm^{-1}, as shown in Figure 4.10. Carbonate species found were similar to those studied using CO_2-DRIFT, as described below. The main difference between the catalyst

samples was the reduction in carbonate species adsorption on the Ru/2Y_2O_3-ZrO_2, Ru/La_2O_3-ZrO_2, and Ru/WO_3-La_2O_3-ZrO_2 catalysts, where the WO_3 based catalyst barely showed any vibration of any carbonate species, similar to the Ru-CO species.

4.5.2 Commercial ZrO_2-based catalysts

CO-DRIFT was also performed on the commercial zirconia-prepared supports and was analysed in the same way as for the co-precipitated supports. The results, illustrated in Figure 4.11, showed that CO adsorption occurred in the same way as in the previous analysis of co-precipitated support catalysts with three main peaks. The peaks were almost identical to those of the co-precipitated supports apart from the Ru/10WO_3-ZrO_2 sample, showing a significant shift in the 2065 cm^{-1} and 2121 cm^{-1} peaks, indicating different molecular vibrations compared to the other samples. The peaks of the Ru/WO_3-ZrO_2 were instead shifted to 2088 cm^{-1} and 2148 cm^{-1}, indicating a significant change in the Ru-CO interactions, probably due to ruthenium bonded to WO_3. The measurements of CO-DRIFT using the Ru/WO_3-ZrO_2 catalyst also showed almost no CO adsorption on neither the Ru or carbonate region, only visible after normalisation of the curve.

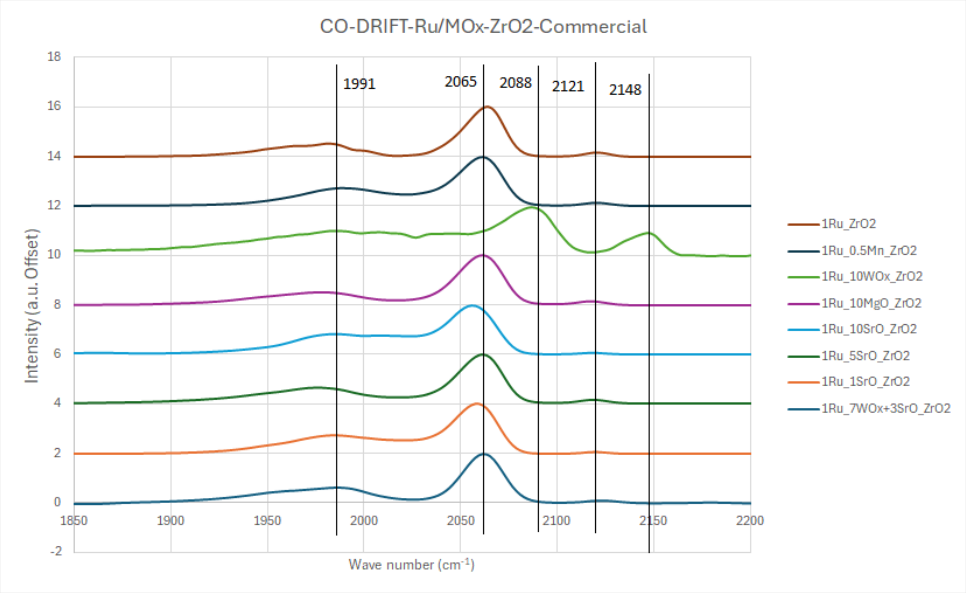

Figure 4.11: CO-DRIFT of a few selected commercial ZrO_2 based catalysts. The general trend is the same with every catalyst except with the WO_3-based ones, highlighted in red.

For a select number of catalysts, CO_2-DRIFTS was also performed to identify carbonate species bonded to the metal oxides of the samples. These were done to analyse the CO_2 adsorption

and bond strength of certain types of carbonate species. The results, illustrated in Figure 4.12, showed that most of the adsorption of CO_2 was found in the form of carbonates, such as bridged, chelated, and carboxylates. The CO_2-DRIFT measurements also showed that a wide range of carbonate species were found adsorbed on the Ru/ZrO_2 catalyst, both strongly and weakly adsorbed, while only a select few strongly adsorbed carbonate species and few weakly adsorbed carbonates were found on the Ru/MgO-ZrO_2 and Ru/SrO-ZrO_2 catalysts. The Ru/WO_3-ZrO_2 catalyst also showed almost no CO_2 adsorption properties, only showing weakly adsorbed carbonates, similar to the DRIFT and CO_2-desorption measurements, which showed almost none CO/CO_2 adsorption.

The carbonate species identified were monodentate carbonate (MDC), chelating bidentate carbonate (CBC), bridged bidentate carbonate (BBC), free carbonates (FC, $CO_3^- M^+$) and carboxylates (CO) [38]. The structure of the carbonates is illustrated in Figure 4.13.

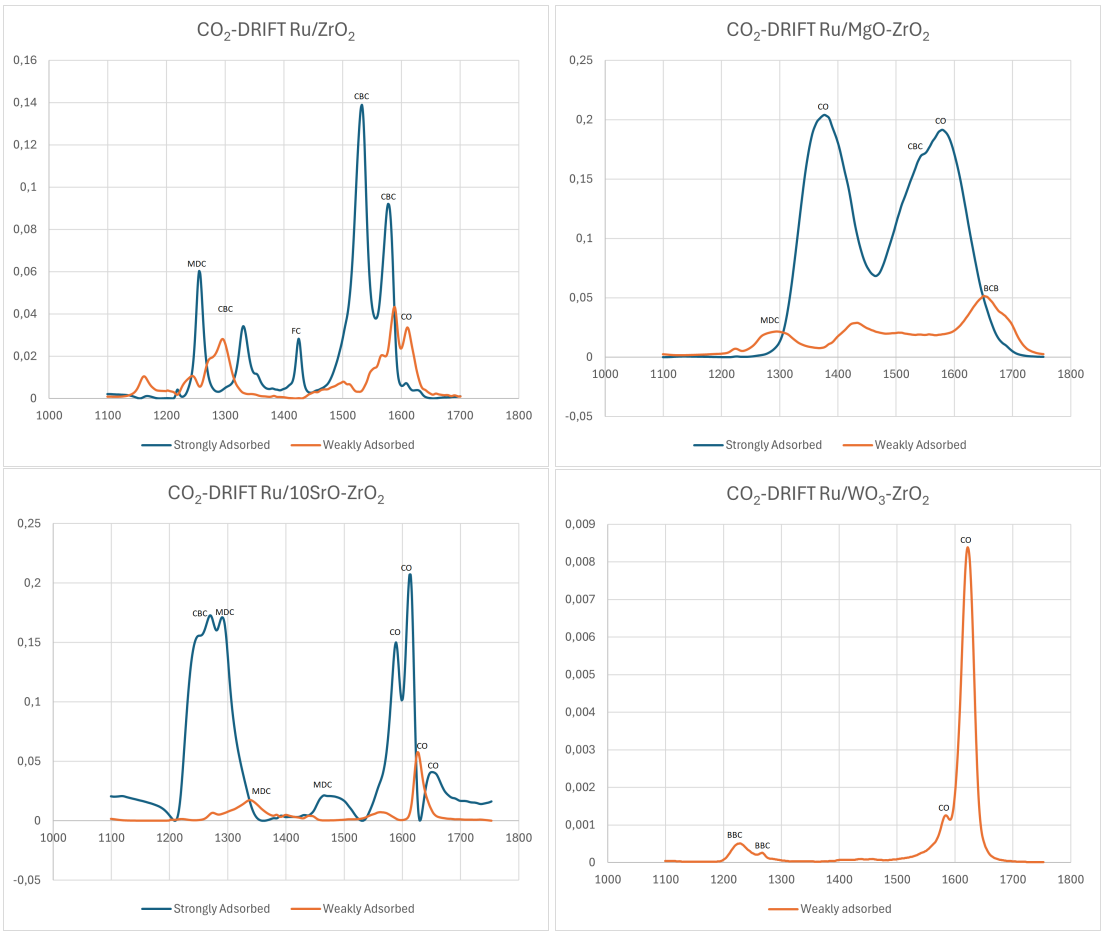

Figure 4.12: CO_2-DRIFT of a select number of commercial ZrO_2 catalysts

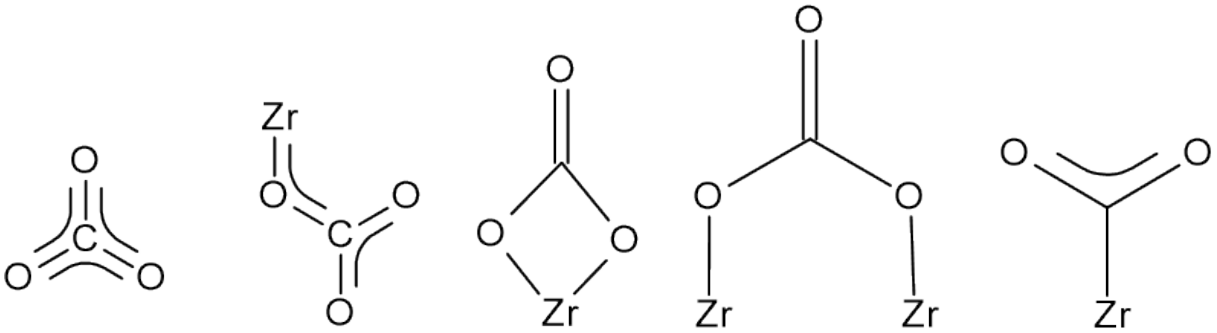

Figure 4.13: The structure of a selection of carbonates found by FTIR methods using CO_2-DRIFT.

4.6 Catalyst depolymerisation activity tests

Based on all previously used catalyst characterization methods, the depolymerisation of nylon 6 to ϵ-caprolactam was tested with conversion (by mass before and after the reaction and filtering of reaction products) as well as the yield of ϵ-caprolactam, as shown in Table 4.4. In the first part of the study, reactions using co-precipitated catalysts showed low conversions ($\leq$ 20%) of nylon 6 to ϵ-caprolactam. This showed that 700°C calcined catalysts or cubic phase zirconia-supported ruthenium catalysts were likely not effective in converting nylon 6 to ϵ-caprolactam, likely due to the smaller surface area of these samples or the extremely low basicity as shown by the CO_2-TPD analysis. This could also be due to the lower than expected MO_x loading, as shown by the ICP-MS analysis, which revealed that the metal loading of most co-precipitated catalysts did not fully meet expectation, especially the Ru/MgO-La_2O_3-ZrO_2 and Ru/SrO-La_2O_3-ZrO_2 catalysts, but also the Ru/WO_3-La_2O_3-ZrO_2 catalyst. Even samples with a larger surface area of the co-precipitated catalysts did not show any increase in conversion. The yttrium stabilized zirconia (YSZ) support was also synthesized and expected to be tested, but due to the low surface area (22,2 $\frac{m^2}{g}$), the catalyst was excluded from activity testing.

Table 4.4: Reaction depolymerisation activity measurements of all catalysts, showing results in the form of conversion and yield, obtained from GC-MS analysis.

Sample	**Conversion (% by mass)**	**Yield (% CL)**
Ru/WO_3-La_2O_3-ZrO_2	12,0	4,7
Ru/MgO-La_2O_3-ZrO_2	12,2	6,5
Ru/SrO-La_2O_3-ZrO_2	16,2	8,6
400Ru/SrO-La_2O_3-ZrO2	20,2	14,1
Commercial ZrO_2 catalysts, 500°C Calcination		
Ru/10% SrO-ZrO_2	42,4	33,8
Ru/5% SrO-ZrO_2	28,8	22,6
Ru/1% SrO-ZrO_2	12,4	6,4
Ru/10% WO_3-ZrO_2	9,8	4,4
Ru/10% MgO-ZrO_2	7,8	3,8
Ru/3% SrO-7% WO_3-ZrO_2	9,0	4,5
Ru/0,5Mn-ZrO_2	19,6	9,4
Ru/ZrO_2	22,6	11,7

In the first part of the depolymerisation tests, the co-precipitated Ru/SrO-La_2O_3-ZrO_2 catalyst showed the greatest promise by the highest conversion of 16,2% and 8,6% CL yields. An even higher conversion of 20,2% and 14,1% CL yield was obtained when the ruthenium precursor was calcined at lower temperature (400 °C vs 500 °C), as shown from the 400Ru/SrO-La_2O_3-ZrO_2 depolymerisation test in Table 4.4. This realization led to the decision to test the commercially available ZrO_2 catalyst with the same focus on the basicity and acidity of the support. The immediate result of the commercial ZrO_2-based catalysts showed an immediate improvement for some catalysts, while a decrease in conversion and yield for others. The Ru/10WO_3-ZrO_2, Ru/10% MgO-ZrO_2 and Ru/3SrO-7WO_3-ZrO_2 showed <10% conversion and <5% CL yield, 50-60% decrease from the most successful 400Ru/SrO-La_2O_3-ZrO2 co-precipitated catalyst. The base case of Ru/ZrO_2 showed a slight increase ($\approx$ 10%) in conversion and a slight decrease ($\approx$ 20%) in CL yield. The Ru/0,5Mn-ZrO_2 catalyst also showed a further 10% decrease in conversion and 20% decrease in CL yield compared to the Ru/ZrO_2 catalyst.

The catalyst with the highest mass conversion was determined to be the Ru/10SrO-ZrO_2 cata-

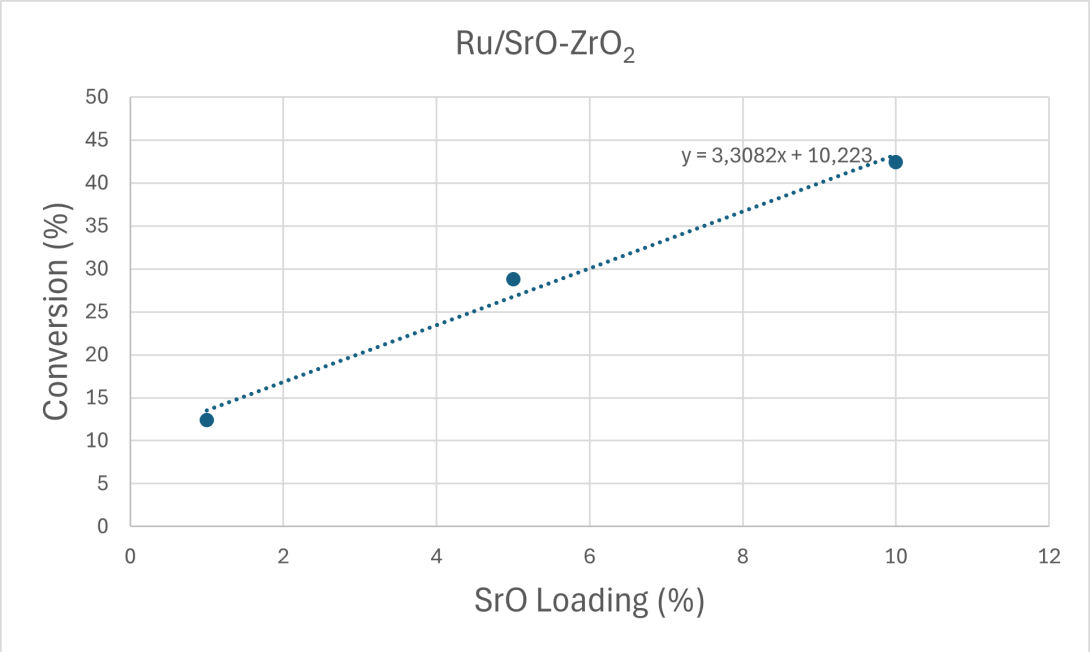

Figure 4.14: The effect of SrO loading on the Ru/SrO-ZrO_2 catalyst between the range of 1-10 wt% SrO loading.

lyst, with a 42,4% conversion and a 33,8% CL yield. Compared to the Ru/ZrO_2 catalyst, this resulted in an 87% increase in conversion and a 189% increase in CL yield. The general trend observed for the conversion of Ru/SrO-ZrO_2 catalysts are shown in Figure **??**. This showed a linear trend between the SrO wt% loadings studied and a possible increasing trend toward higher loadings. However, this trend is difficult to prove with the limited amount of depolymerization activity tests performed using the Ru/SrO-ZrO_2 catalysts and no knowledge of further trends beyond 10% by weight of SrO.

Although no other products other than ϵ-caprolactam were found by GC-MS analysis, the discrepancy between conversion and yield to caprolactam was mainly due to the unrecoverable solid nylon 6 stuck to other parts of the reactor that could not be measured. Some of the discrepancy could also be due to the formation of gas phase products, which were not analysed during the study.

Although there was generally a low yield for most reactions, the few reactions that worked proved an important point, the simplicity of the separation of the ϵ-caprolactam product. A simple vacuum filtration system of the hexadecane solvent was able to separate ϵ-caprolactam, as shown in Figure 4.15.

Figure 4.15: The resulting caprolactam after reaction using the Ru/10Sr-ZrO_2 catalyst, showing the ease of filtration of the caprolactam

The representation of the results, shown in Figure 4.16, shows that the catalysts most successful in the hydrogenative depolymerisation of nylon-6 were the Ru / 10SrO-ZrO_2 catalyst by a large margin, where the stronger basic sites and some acidic sites of the catalyst showed a great impact on catalytic efficiency, as shown in the TPD measurements. The increase in SSA did not significantly affect the catalytic efficiency as previously hypothesized, as can be seen with the lower SSA ($\approx$ 12%) of the Ru/10SrO-ZrO_2 catalyst compared to the Ru/5SrO-ZrO_2 catalyst while showing a marginally higher conversion of nylon-6. The co-precipitation of the MO_x-ZrO_2 support also did not seem to induce the basic and acidic sites, but rather weaken them, or completely block them, as shown by the almost non-existent CO_2 desorption of the co-precipitated catalysts. However, whether this trend would still occur had the co-precipitated supports precipitated fully is still unknown.

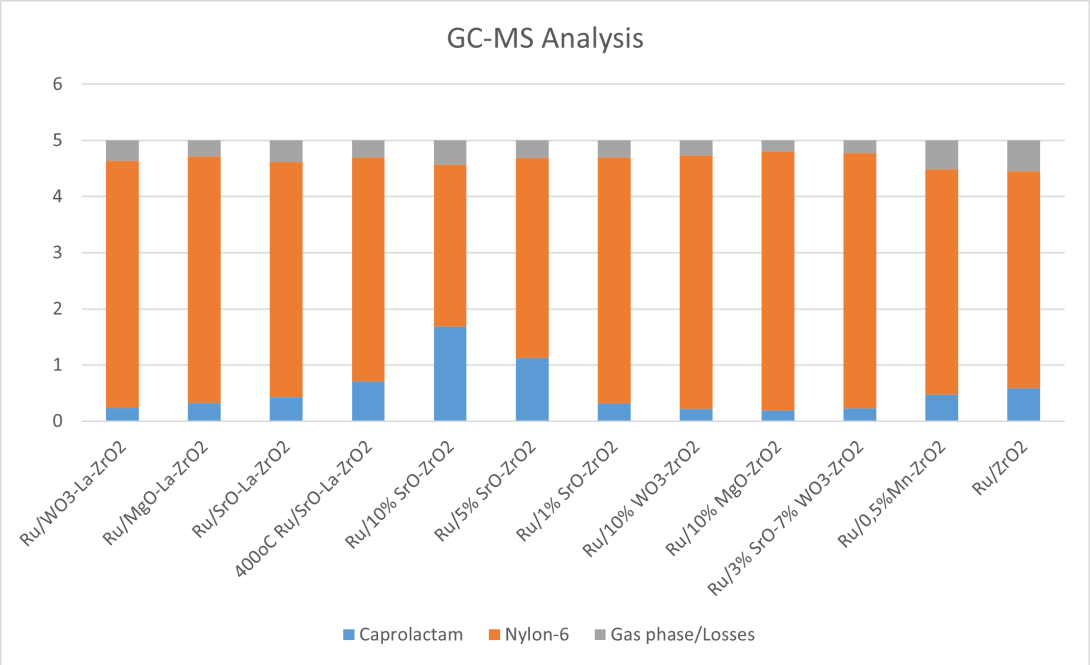

Figure 4.16: Overall conversion and fractions of solid, liquid and gas/losses of catalytic depolymerisation.

5

Conclusion

The results of the study showed some promising alternatives for the catalytic depolymerisation of nylon-6 into ϵ-caprolactam. The addition of acidic WO_3 did not appear to increase the yield or conversion of the depolymerisation of nylon-6, but rather hinder the ability to convert nylon 6 and reduced, rather than increased, the amount of acidic sites, as shown in the NH_3-TPD studies. However, with the addition of basic metal oxides, whereas MgO and SrO were tested, the amount of basic sites increased. The highest number of basic sites and highest conversion in the depolymerisation test was shown by the catalysts Ru/10SrO-ZrO_2 and Ru/5SrO-ZrO_2. The Ru/SrO-ZrO_2 catalysts also showed a steady increase in strong basic sites with increased SrO loading, probably indicating the strong influence of strong basic sites on the conversion of nylon 6 to ϵ-caprolactam.

The highest conversion and yield achieved was by the Ru/10SrO-ZrO_2 catalyst with 42,4% conversion and 33,8% yield. This showed that the increase in strong basic sites has a large effect on the catalytic depolymerisation of nylon 6. The biggest difference from the Ru/10SrO-ZrO_2 catalyst was that it also showed signs of starting to form a completely new crystallographic phase, the orthorhombic perovskite $SrZrO_3$ crystal structure. This crystal structure did not show in any other catalyst samples, and the increase in SrO could even contribute to further crystallization of the perovskite $SrZrO_3$ phase. Whether this increase in SrO loading would potentially impact conversion is still unknown.

5.1 Further studies

Based on the results and conclusions of the study, many questions were answered, but more questions could always be asked, such as whether increasing the SrO loading beyond 10% by weight would further increase the conversion of nylon 6 of the hydrogenative depolymerisation

reaction. The effect of increased/decreased ruthenium loading was also not investigated and could have proven effective in increasing the conversion of the depolymerisation reaction.

Due to the success of the Ru/10SrO-ZrO_2 catalyst and the introduction of the orthorhombic perovskite $SrZrO_3$ phase on the same catalyst, other perovskites could also be investigated as potential support material, such as calcium titanium oxide ($CaTiO_3$) or different configurations of $SrZrO_3$-ZrO_2 supports. Studies on increasing the reliability of co-precipitated MO_x-ZrO_2 supports could also be investigated to show the precipitation conditions of such supports.

Bibliography

[1] Hannah Ritchie, Veronika Samborska, and Max Roser. *Plastic Pollution*. Accessed: 2025-05-22. 2023. URL: https://ourworldindata.org/plastic-pollution.

[2] Science History Institute. *History and Future of Plastics*. Accessed: 2025-05-22. 2025. URL: https://www.sciencehistory.org/education/classroom-activities/role-playing-games/case-of-plastics/history-and-future-of-plastics/.

[3] Statista Research Department. *Annual Production of Plastics Worldwide from 1950 to 2022*. Accessed: 2025-06-05. 2023. URL: https://www.statista.com/statistics/282732/global-production-of-plastics-since-1950/.

[4] Hannah Ritchie, Veronika Samborska, and Max Roser. *Plastic Pollution*. https://ourworldindata.org/plastic-pollution?insight=only-a-small-share-of-plastic-gets-recycled#key-insights. Accessed: 2025-06-05. 2023. URL: https://ourworldindata.org/plastic-pollution?insight=only-a-small-share-of-plastic-gets-recycled%5C#key-insights.

[5] Zoé O. G. Schyns and Michael P. Shaver. "Mechanical Recycling of Packaging Plastics: A Review". In: *Macromolecular Rapid Communications* 42.3 (2021). Accessed: 2025-05-22, p. 2000415. DOI: https://doi.org/10.1002/marc.202000415. URL: https://onlinelibrary.wiley.com/doi/abs/10.1002/marc.202000415.

[6] Jung Eun Lee et al. "Current methods for plastic waste recycling: Challenges and opportunities". In: *Chemosphere* 370 (2025). Accessed: 2025-05-22, p. 143978. ISSN: 0045-6535. DOI: https://doi.org/10.1016/j.chemosphere.2024.143978.

URL: https://www.sciencedirect.com/science/article/pii/S0045653524028868.

[7] Pantelis G. Nikolakopoulos and Angelos P. Markopoulos. “Editorial on simulation and modeling using digital twins in mechanical design and in advanced manufacturing technology”. In: *Simulation Modelling Practice and Theory* 133 (2024). Accessed: 2025-06-19, p. 102904. ISSN: 1569-190X. DOI: 10.1016/j.simpat.2024.102904.

[8] Ana C. Fernandes. “Reductive depolymerization as an efficient methodology for the conversion of plastic waste into value-added compounds”. In: *Green Chem.* 23 (19 2021). Accessed: 2025-05-22, pp. 7330–7360. DOI: DOI:10.1039/D1GC01634B. URL: http://dx.doi.org/10.1039/D1GC01634B.

[9] Prabin Dhakal. “Catalysts for depolymerization of nylon-6 to ε-caprolactam - insights into activity-structure relationships”. Licentiate thesis. Gothenburg, Sweden: Chalmers, June 2025.

[10] Jian Chen et al. “Metal–support interactions for heterogeneous catalysis: mechanisms, characterization techniques and applications”. In: *J. Mater. Chem. A* 11 (16 2023). Accessed: 2025-06-03, pp. 8540–8572. DOI: 10.1039/D2TA10036C. URL: http://dx.doi.org/10.1039/D2TA10036C.

[11] Sebastian Cisneros et al. “The effect of O-vacancies on intermediates stability and electron delocalization over MgO modified Ru/ZrO_2: Spectroscopic insights during CO2 methanation”. In: *Chemical Engineering Journal* 474 (2023). Accessed: 2025-01-27. URL: https://doi.org/10.1016/j.cej.2023.145646.

[12] K. Foger. “Dispersed Metal Catalysts”. In: *Catalysis: Science and Technology Volume 6*. Ed. by John R. Anderson and Michel Boudart. Accessed: 2025-05-26. Berlin, Heidelberg: Springer Berlin Heidelberg, 1984, pp. 227–305. ISBN: 978-3-642-93250-2. DOI: 10.1007/978-3-642-93250-2_4. URL: https://doi.org/10.1007/978-3-642-93250-2_4.

[13] Manabu Miyamoto et al. “Effect of basicity of metal doped ZrO2 supports on hydrogen production reactions”. In: *International Journal of Hydrogen Energy* 43.2 (2018). Accessed: 2025-01-27, pp. 730–738. URL: https://doi.org/10.1016/j.ijhydene.2017.11.041.

[14] U.S. Department of Energy. *DOE Explains...Catalysts*. Accessed: 2025-06-13. 2025. URL: https://www.energy.gov/science/doe-explainscatalysts.

[15] Hasa. *What is the Difference Between Heterogeneous and Homogeneous Catalyst*. Accessed: 2025-06-13. 2023. URL: https://pediaa.com/what-is-the-difference-between-heterogeneous-and-homogeneous-catalyst/.

[16] Primidi. *Catalysis - Inhibitors, Poisons and Promoters*. Accessed: 2025-05-26. 2024. URL: https://www.primidi.com/catalysis/inhibitors_poisons_and_promoters.

[17] Huazhang Liu. "Ammonia synthesis catalyst 100 years: Practice, enlightenment and challenge". In: *Chinese Journal of Catalysis* 35.10 (2014). Accessed: 2025-06-10, pp. 1619–1640. ISSN: 1872-2067. DOI: https://doi.org/10.1016/S1872-2067(14)60118-2. URL: https://www.sciencedirect.com/science/article/pii/S1872206714601182.

[18] XUE-CHAO HU and H.H. YANG. "1.11 - Polyamide and Polyester Fibers". In: *Comprehensive Composite Materials*. Ed. by Anthony Kelly and Carl Zweben. Accessed: 2025-05-10. Oxford: Pergamon, 2000, pp. 327–344. ISBN: 978-0-08-042993-9. DOI: https://doi.org/10.1016/B0-08-042993-9/00060-7. URL: https://www.sciencedirect.com/science/article/pii/B0080429939000607.

[19] Amit Kumar et al. "Hydrogenative Depolymerization of Nylons". In: *Journal of the American Chemical Society* 142.33 (2020). Accessed: 2025-05-26, pp. 14267–14275. DOI: 10.1021/jacs.0c05675. URL: https://doi.org/10.1021/jacs.0c05675.

[20] Bahareh A.T. Mehrabadi et al. *Advances in Catalysis*. Accessed: 2025-01-29. Academic Press, 2017. ISBN: 9780128120781. URL: https://doi.org/10.1016/bs.acat.2017.10.001.

[21] Peter Munnik, Petra E. de Jongh, and Krijn P. de Jong. "Recent Developments in the Synthesis of Supported Catalysts". In: *Chemical Reviews* 115.14 (2015). Accessed: 2025-02-04, pp. 6687–6718. URL: https://doi.org/10.1021/cr500486u.

[22] Carl Lundstedt. *BET Theory and how its used to calculate surface area*. Accessed: 2025-02-20. June 2019. URL: https://static.horiba.com/fileadmin/Horiba/Products/Scientific/Particle_Characterization/Webinars/Slides/BET_Theory_Explained.pdf.

[23] Stephen Brunauer, P. H. Emmett, and Edward Teller. "Adsorption of Gases in Multimolecular Layers". In: *Journal of the American Chemical Society* 60.2 (1938). Accessed:

2025-03-07, pp. 309–319. DOI: 10.1021/ja01269a023. URL: https://doi.org/10.1021/ja01269a023.

[24] Encyclopædia Britannica. *X-ray diffraction*. Accessed: 2025-03-15. 2025. URL: https://www.britannica.com/science/X-ray-diffraction.

[25] Z. Liu et al. "Surface acidity and basicity of mixed metal oxide supports". In: *Applied Surface Science* 127.1 (1998). Accessed: 2025-05-26, pp. 1–7. DOI: 10.1016/S0920-5861(98)00047-9. URL: https://doi.org/10.1016/S0920-5861(98)00047-9.

[26] A. Rukini et al. "Metals Production and Metal Oxides Reduction Using Hydrogen: A Review". In: *Journal of Sustainable Metallurgy* 8.1 (Jan. 2022). Accessed: 2025-05-26, pp. 1–24. DOI: 10.1007/s40831-021-00486-5. URL: https://doi.org/10.1007/s40831-021-00486-5.

[27] D. Ugur et al. "Kinetics of Reduction of a RuO2(110) Film on Ru(0001) by H2". In: *The Journal of Physical Chemistry C* 116.51 (2012). Accessed: 2025-06-10, pp. 26822–26828. DOI: 10.1021/jp309905z. URL: https://doi.org/10.1021/jp309905z.

[28] Carlo Pirola, Federico Galli, and Gregory S. Patience. "Experimental methods in chemical engineering: Temperature programmed reduction—TPR". In: *The Canadian Journal Of Chemical Engineering* 96 (2018). Accessed: 2025-03-11, pp. 2317–2320. ISSN: 11. DOI: https://doi.org/10.1002/cjce.23317. URL: https://onlinelibrary.wiley.com/doi/full/10.1002/cjce.23317?msockid=2140a98333856f6f0799bcff32ee6e4f.

[29] Mark B. Mitchell. "Fundamentals and Applications of Diffuse Reflectance Infrared Fourier Transform (DRIFT) Spectroscopy". In: *Structure-Property Relations in Polymers*. Accessed: 2025-04-07. ACS Publications, 1993. Chap. 13, pp. 351–375. DOI: 10.1021/ba-1993-0236.ch013. URL: https://pubs.acs.org/doi/abs/10.1021/ba-1993-0236.ch013.

[30] Feiyi Zhou et al. "Efficient catalytic oxidation of chlorinated volatile organic compounds over RuO2-WOx/Sn0.2Ti0.8O2 catalysts: Insight into the Cl poisoning mechanism of acid sites". In: *Chemical Engineering Journal* 464 (2023). Accessed: 2025-06-12, p. 142471. ISSN: 1385-8947. DOI: https://doi.org/10.1016/j.

cej.2023.142471. URL: https://www.sciencedirect.com/science/article/pii/S1385894723012020.

[31] D. Padmakar et al. “Understanding the role of SrO-ZrO2 mixed oxide support for Co3O4 based catalysts towards H2 production from steam reforming of glycerol”. In: *Applied Surface Science* 606 (2022). Accessed: 2025-06-06, p. 154954. ISSN: 0169-4332. DOI: https://doi.org/10.1016/j.apsusc.2022.154954. URL: https://www.sciencedirect.com/science/article/pii/S0169433222024825.

[32] Yougui Liao. *SrZrO3*. Accessed: 2025-06-12. 2006. URL: https://www.globalsino.com/EM/page1872.html.

[33] J. C. Slater. “Atomic Radii in Crystals”. In: *Journal of Chemical Physics* 41 (1964). Accessed: 2025-06-19, pp. 3199–3205. ISSN: 10. DOI: doi:10.1063/1.1725697.

[34] Zeid Alothman. “A Review: Fundamental Aspects of Silicate Mesoporous Materials”. In: *Materials* 5 (Dec. 2012). Accessed: 2025-06-19, pp. 2874–2902. DOI: 10.3390/ma5122874.

[35] Eveliina Mäkelä et al. “Hydrodeoxygenation of Levulinic Acid Dimers on a Zirconia-Supported Ruthenium Catalyst”. In: *Catalysts* 10 (Feb. 2020). Accessed: 2025-04-12, p. 200. DOI: 10.3390/catal10020200.

[36] Yujing Li, Tao Qin, and Yan Wei. “A Single Site Ruthenium Catalyst for Robust Soot Oxidation Without Platinum or Palladium”. In: *Nature Communications* 14 (2023). Accessed: 2025-05-16, p. 7149. DOI: 10.1038/s41467-023-42935-7. URL: https://doi.org/10.1038/s41467-023-42935-7.

[37] Xiuyun Wang et al. “Atomically Dispersed Ru Catalyst for Low-Temperature Nitrogen Activation to Ammonia via an Associative Mechanism”. In: *ACS Catalysis* 10.16 (2020). Accessed on 2025-05-31, pp. 9504–9514. DOI: 10.1021/acscatal.0c00549.

[38] Jiaxiong Liu et al. “Transformation of CO2 and glycerol to glycerol carbonate over CeO2ZrO2 solid solution —— effect of Zr doping”. In: *Biomass and Bioenergy* 118 (2018). Accessed: 2025-06-03, pp. 74–83. ISSN: 0961-9534. DOI: https://doi.org/10.1016/j.biombioe.2018.08.004. URL: https://www.sciencedirect.com/science/article/pii/S0961953418302009.

A

Appendix 1

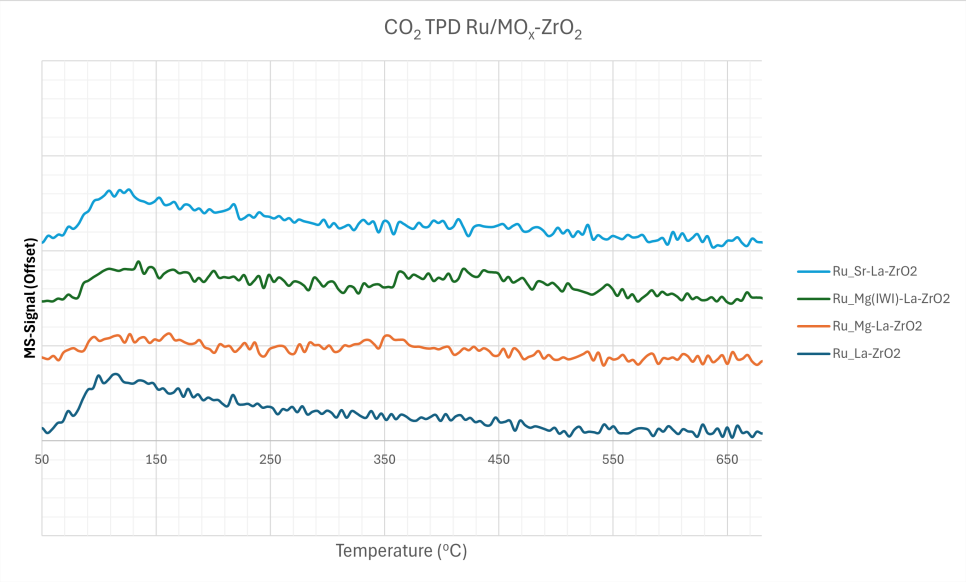

Figure A.1: CO_2-TPD measurement of synthesised catalysts, showing low to no desorption apart from a small peak at 110°C.

DEPARTMENT OF CHEMISTRY AND CHEMICAL ENGINEERING

CHALMERS UNIVERSITY OF TECHNOLOGY

Gothenburg, Sweden

www.chalmers.se

CHALMERS
UNIVERSITY OF TECHNOLOGY